ADVANCED THEORY AND SIMULATIONS
www.advtheorysimul.com

Pharmacophore-Based Modeling, Synthesis, and Biological Evaluation of Novel Quinazoline/Quinoline Derivatives: Discovery of EGFR Inhibitors with Low Nanomolar Activity

Asaf Evrim Evren, Begüm Nurpelin Sağlik Özkan, Gülşen Akalin-Çiftçi, and Leyla Yurttaş*

The main aim of this study is to obtain novel molecules that are more selective on cancer cells compared to healthy cells. For this purpose, four hit molecules are identified using 11 new pharmacophore hypotheses followed by scanning the in-house database. Then, based on those hit molecules, the synthesis and analysis of four different series (three quinazolines and one quinoline series) are carried out, and their anticancer activity is investigated. Finally, by using molecular docking and dynamics simulation methods, binding mode and structure–activity relationship are examined. Among the quinazolin-4(*3H*)-one derivatives, those containing halogen atom are found to be potentially effective, while the best epidermal growth factor receptor (EGFR) inhibition and apoptosis induction are displayed by compounds containing 4-amino-1,2,4-triazole moiety. Notably, four compounds (4h, 8d, 8l, and 8m) show EGFR inhibition activity at 5.298 ± 0.164, 5.46 ± 0.221, 2.670 ± 0.124, and 2.191 ± 0.908 × 10^{-9} M, their inhibitory activity is similar to or stronger than gefitinib (IC_{50}: 4.169 ± 0.156 × 10^{-9} M). In addition, EGFR inhibitor concentration of 4g, 8e, and 8o is determined as 27588 ± 6.945, 52.41 ± 2.312, and 33657 ± 8.512 × 10^{-9} M. These findings indicate that generated pharmacophore hypotheses successfully determine new EGFR inhibitors. In conclusion, four novel compounds, more active than gefitinib with fewer side effects, are reached, and the structure–activity relationships are clarified.

1. Introduction

Cancer, described simply as the uncontrolled proliferation of cells, is a name given to a very wide family of diseases that can affect a wide variety of organs and tissues individually or together.[1] The treatment varies according to dynamic protocols, considering the type of cancer, and patient-specific personal characteristics such as age and gender. The treatment options are currently grouped under four classes. These are surgical,[2] radiotherapy,[3] chemotherapy,[4] and immunotherapy;[5] however, two or more approaches can be applied together or sequentially during treatment.[6,7] In recent years, the rapid increase in lung cancer cases and related mortality rates has been a serious warning for the world.[8–10] In addition, the deterioration of treatment efficacy because of resistance to conventional chemotherapeutics[11–15] resulted in an urgent need for the development of alternative novel therapies.[16] Thus, the aims of this study are to obtain compounds with selective cytotoxicity on cancer cells, figure out their mechanism of action, and reveal their structure–effect relationships. For this purpose, the epidermal growth factor receptor (EGFR) was determined as the target protein when the lung cancer cases were examined.

Receptor tyrosine kinases (RTKs), members of the tyrosine kinases family, play an important role in the regulation of cell growth, survival, and cell differentiation.[17] Overexpression has been observed in a wide variety of human cancer cells, including breast, ovarian, colon, and non-small lung cancers. Among RTKs, EGFR, also named HER1, is an important drug target that has been extensively studied.[18,19] As one of four members of the ErbB family, EGFR-tyrosine kinase has been confirmed as one of the most effective targets for the treatment of non-small cell lung cancer (NSCLC).[20–22] So far, thousands of EGFR tyrosine kinase inhibitors (EGFR-TKI) have been synthesized and evaluated. The mechanism underlying EGFR inhibition is occupying the ATP-binding site of tyrosine kinase (EGFR-TK), which prevents small molecules from being autophosphorylated. This inhibits signal transduction, which in turn suppresses the growth of tumor cells.[23,24] However, despite remarkable progress in the

A. E. Evren
Vocational School of Health Services
Department of Pharmacy Services
Bilecik Şeyh Edebali University
Bilecik 11000, Turkey
E-mail: asafevrimevren@anadolu.edu.tr

A. E. Evren, B. N. Sağlik Özkan, L. Yurttaş
Faculty of Pharmacy
Department of Pharmaceutical Chemistry
Anadolu University
Eskişehir 26470, Turkey

G. Akalin-Çiftçi
Faculty of Pharmacy
Department of Biochemistry
Anadolu University
Eskişehir 26470, Turkey

DOI: 10.1002/adts.202400811

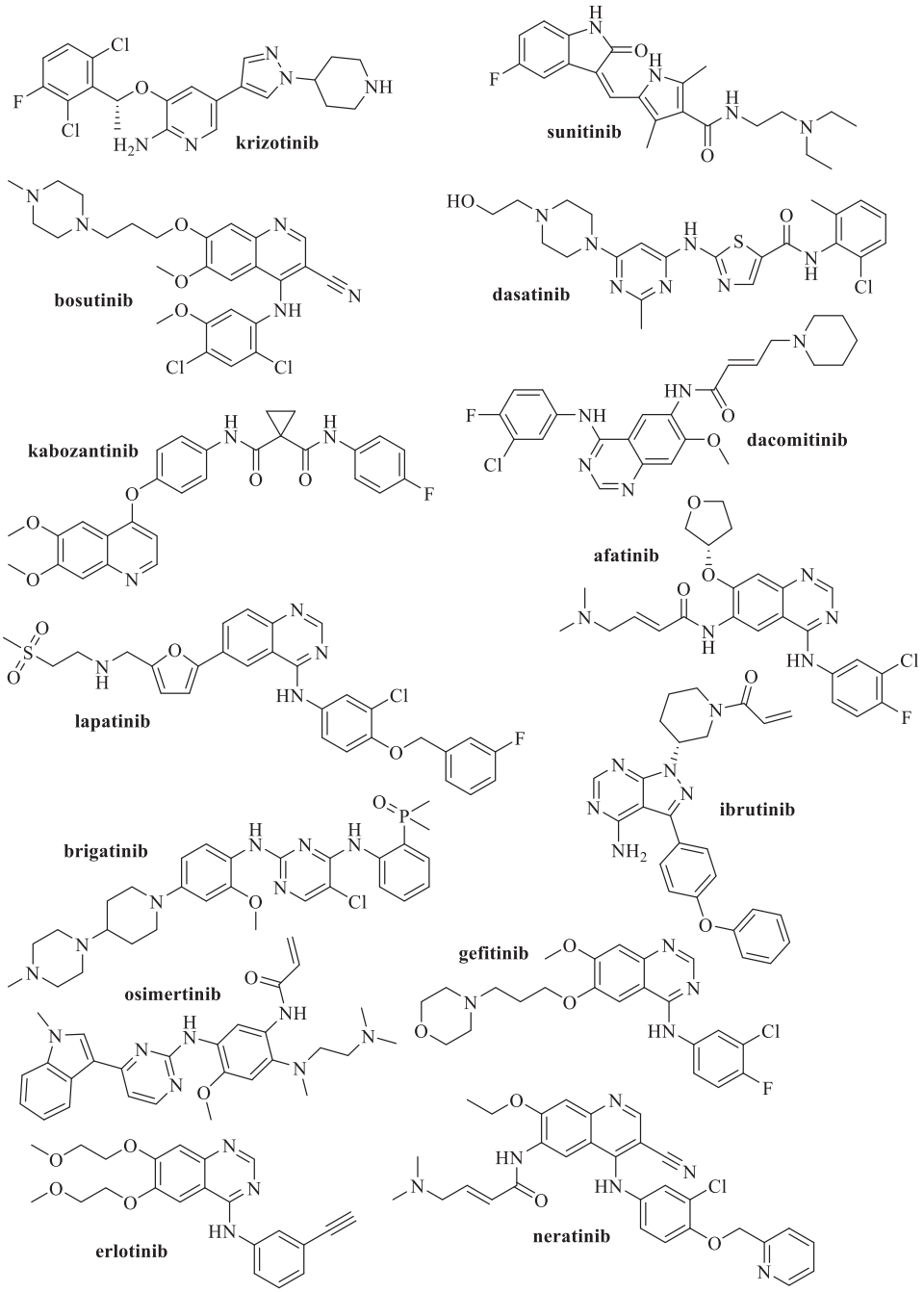

Figure 1. EGFR inhibitors.

clinical treatment of non-small cell lung cancer, the development of drug resistance and dose toxicity greatly limit the persistence of the therapeutic effect.[25] Therefore, the primary goal is that the cytotoxic activity of the new developed molecule is selective to cancer cells.

Upon examining the structure of the compounds that have been developed for EGFR inhibition so far,[26] nitrogen-containing ring compounds stand out, and drugs with rings of pyridine/pyrimidine and their benzene condensed analogs, quinoline/quinazoline, are prominent. Although condensed pyrimidine ring systems with different cyclic structures are also observed, the quinazoline ring system stands out as the most striking structure with the effect of its clinically used analogs. Among them, gefitinib and erlotinib are known as first-generation EGFR inhibitors while afatinib, neratinib, and dacomitinib are known as second-generation EGFR inhibitors. All EGFR inhibitors are shared in **Figure 1**.

In addition to that, the quinazoline ring has various pharmacological activities such as A_{2A} adenosine receptor antagonist,[27] cytokine inhibition,[28] antibacterial,[29] antifungal,[30,31] anti-inflammatory,[32] antimycobacterial,[33] antiviral,[34] and anti-cancer effect.[35–40]

Table 1. Validation parameters of the suitable hypotheses.

HypoNo	Phase Hypo Score	EF1%	BEDROC ($\alpha = 20$)	ROC	AUAC	RIE
DHHRRR_1	1.03	48.64	0.867	0.86	0.92	14.22
DHRRR_3	1.19	48.64	0.819	0.79	0.88	13.43

Note: **D**: Hydrogen bond donor, **H**: Hydrophobicity, **R**: Ring

In light of the above information, various hypotheses were developed to screen in-house molecule bank which includes designed quinazoline- and quinoline-based molecules. Hit molecules and their analogs were synthesized and analyzed. Their anticancer profiles were investigated through in vitro and in silico approaches. Also their structure–activity relationship (SAR) was clarified.

2. Results and Discussion

2.1. Pharmacophore Hypotheses Studies

Pharmacophore hypotheses were obtained by using two different methods. The first method (Section 5.1.1) was created using both clinically used EGFR (ErbB-1) inhibitors and anticancer drugs (-tinib) that show their anticancer effect through different tyrosine kinase inhibition. The goal here is to exclude compounds that do not interact with ErbB-1 even though they have tyrosine kinase effects, or that may interact weakly. On the other hand, the second method (Section 5.1.2) has collected compounds that have either pyridine or pyrimidine nuclei that show EGFR inhibitory activity from all scientific literature. It is planned to apply the pharmacophore hypotheses derived from these compounds in the screening of in-house molecule banks. Lead compounds were identified using the hypotheses derived from the two methods, and they were then synthesized along with their analogs.

2.1.1. Validation of the hypotheses

Multiple Drugs and One Protein: Among 30 hypotheses that were obtained utilizing drug molecules (first method), only two hypotheses can be used for virtual screening due to the validation data. Confirmation data for these two hypotheses are given in **Table 1**.

The hypotheses DHHRRR_1 and DHRRR_3 evolved out of neratinib (quinoline) and gefitinib (quinazoline) as model molecules, respectively. The 3D representations of the hypotheses are shared in **Figure 2**.

Literature-Based EGFR Inhibitors and One Protein: Among 30 hypotheses obtained using EGFR inhibitors (second method), nine hypotheses can be used for virtual screening due to the validation data. Confirmation data for these nine hypotheses are given in **Table 2**. Also the 3D representations are given in **Figure 3**.

Table 2. Validation parameters of the suitable hypotheses.

Hypo No	Phase Hypo Score	EF1%	BEDROC ($\alpha = 20$)	ROC	AUAC	RIE
AAARR_4	1.21	44.48	0.953	0.96	0.96	15.36
AAAARR_2	1.23	44.48	0.949	0.96	0.96	15.28
AAARR_5	1.20	44.48	0.942	0.96	0.96	15.18
AAARR_2	1.21	44.48	0.947	0.95	0.96	15.25
AAARR_3	1.20	44.48	0.940	0.95	0.96	15.15
AAARRR_3	1.20	44.48	0.922	0.95	0.96	14.85
AAARR_6	1.17	44.48	0.912	0.95	0.96	14.69
AARRR_2	1.13	44.48	0.874	0.95	0.95	14.07
AARRR_1	1.09	44.48	0.831	0.94	0.94	13.38

Note: **A**: Hydrogen bond acceptor, **D**: Hydrogen bond donor, **H**: Hydrophobicity, **R**: Ring

Table 3. Number of in-house molecule data molecules that fit pharmacophore-based hypotheses.

Hypothesis no.	Reference molecule	Number of hit molecules
DHHRRR_1	Neratinib	15
DHRRR_3	Gefitinib	4
AAARR_4	ZINC000096933670	0
AAAARR_2	ZINC000096933693	20
AAARR_5	ZINC000096933693	2
AAARR_2	ZINC000096933669	1
AAARR_3	ZINC000096933670	2
AAARRR_3	ZINC000096933693	11
AAARR_6	ZINC000096933693	4
AARRR_2	ZINC000096933693	0
AARRR_1	ZINC000096933693	0

Note: **A**: Hydrogen bond acceptor, **D**: Hydrogen bond donor, **H**: Hydrophobicity, **R**: Ring

2.1.2. Screening of In-House Data Bank

Total 11 hypotheses were used to screen the in-house molecule bank consisting of novel quinoline or quinazoline derivatives. In this screening process, the matching criteria were set to at least five features within the maximum tolerance area of 2.00 Å for each hypothesis. According to screening results, the reference molecule and hypothesis codes are presented in **Table 3**, and also 3D superimposed of the compatible compounds in the data library is shared in **Figure 4**.

There is no hit molecule for hypotheses AAARR_4, AARRR_2, and AARRR_1. On the contrary, there are 15 and 20 hit compounds for hypotheses DHHRRR_1 and AAAARR_2 (**Figure 4A,C**), respectively. It was observed that these hit compounds were selected due to the presence of *N*-amino triazole moiety which fulfills the criteria of the two hypotheses; however, it seems that the substituent effect is insignificant. Therefore, two opposing questions were raised, is this moiety an essential pharmacophore structure for candidate EGFR inhibitors, or is it the result of a nonselective hypothesis due to the lack of one or more properties? Depending on the calculated external volume for both hypotheses and the presence of 4-amino-1,2,4-triazole derivatives in other hypotheses, the answer for these questions is that this 4-amino-1,2,4-triazole moiety is considered a pharmacophore group. However, in future investigations, it is recommended to either avoid using these two hypotheses

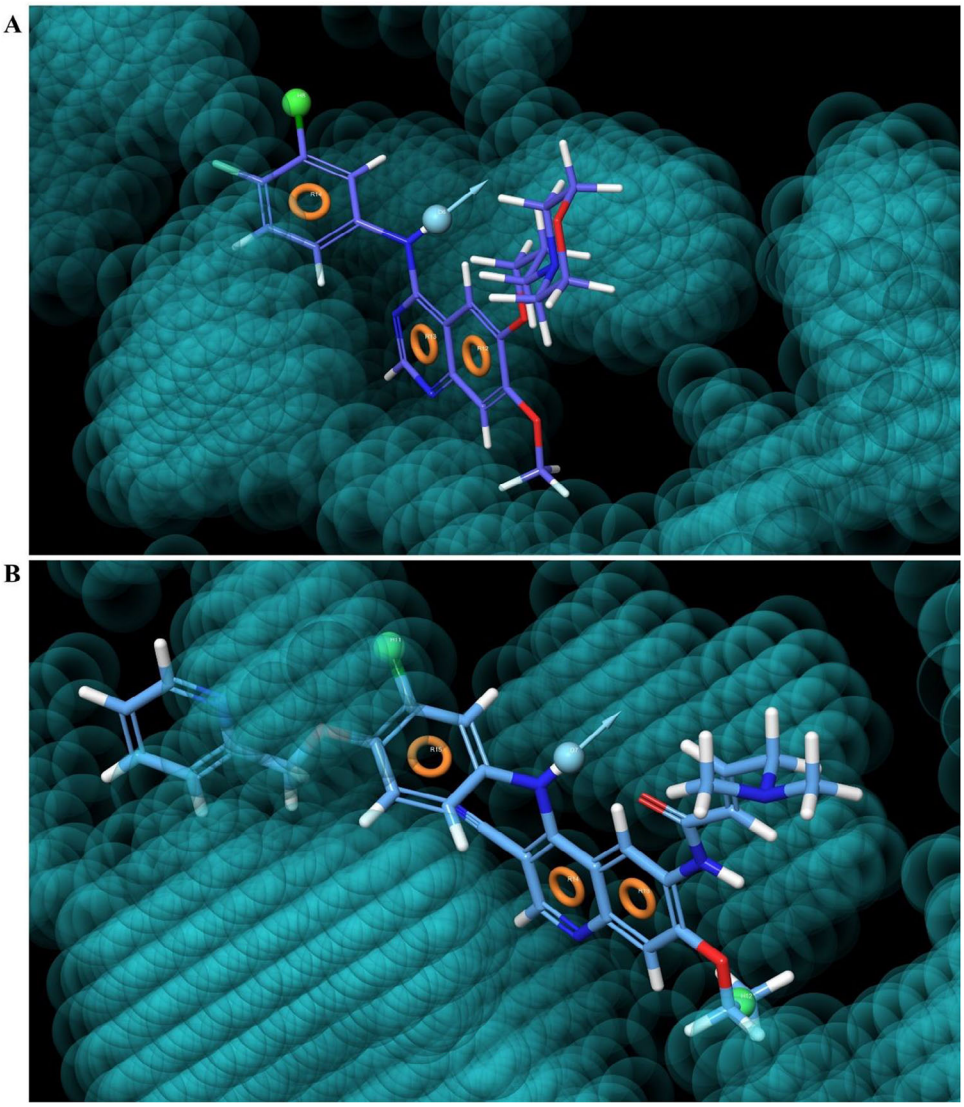

Figure 2. 3D representation of hypotheses DHRRR_3 (top, gefitinib) and DHHRRR_1 (bottom, neratinib). *Blue bubbles represent external volume.

for screening libraries containing 4-amino-1,2,4-triazole and/or its analogs and/or its bioisosteric structures or to use these two hypotheses for a preliminary screening of large databanks. Within the scope of this study, these two hypotheses' models were categorized as secondary since they are not distinctive for 4-amino-1,2,4-triazole derivatives. 3D representations of the hit molecule(s) detected by other hypotheses are shown in Figure 4.

As a result, considering hit molecules, the synthesis of (benzo)thiazoles or hydrazinocarbothioamide moieties attached to *N*-(4-methoxyphenyl)triazole and 4-amino-1,2,4-triazole structures which connected to the third position of the quinazolin-4(*3H*)-one ring by a methylene bridge was carried out. In addition, it was also decided to synthesize *N*-(4-methoxyphenyl)triazole-thiazole derivatives connected by the methyleneoxy bridge to the eighth position of quinoline. These compounds meet the criteria in Section 5.1, and the detected hits and their analogues were taken to the synthesis phase to evaluate their anticancer activities as well as analyze the SARs.

2.2. Chemistry

The lead molecules and their analogues (**Tables 4** and **5**) were synthesized as described in **Scheme 1**. The analyzed spectra of the final compounds are shared in Figure S1.1–S1.120, Supporting Information).

According to ^{1}H-NMR spectra, aromatic hydrogens of molecules within series **4** and **8** were observed at 6.91–8.49 ppm while aromatic hydrogens of molecules within series **13** were at 7.42–8.87 ppm. For the common structure, hydrogens of the CH_2 were observed at 4.78–5.25 ppm. In conclusion, ^{1}H-NMR data of all synthesized compounds were found to be compatible with literature data.[41–44]

According to ^{13}C-NMR spectra, identical peaks between derivatives of the common quinazoline ring were examined and assigned for each carbon. The expected numbers of peaks were obtained for the total carbon number of each compound. Since compounds **4j**, **8a**, and **8l** contain fluoro atom, the spectra of these

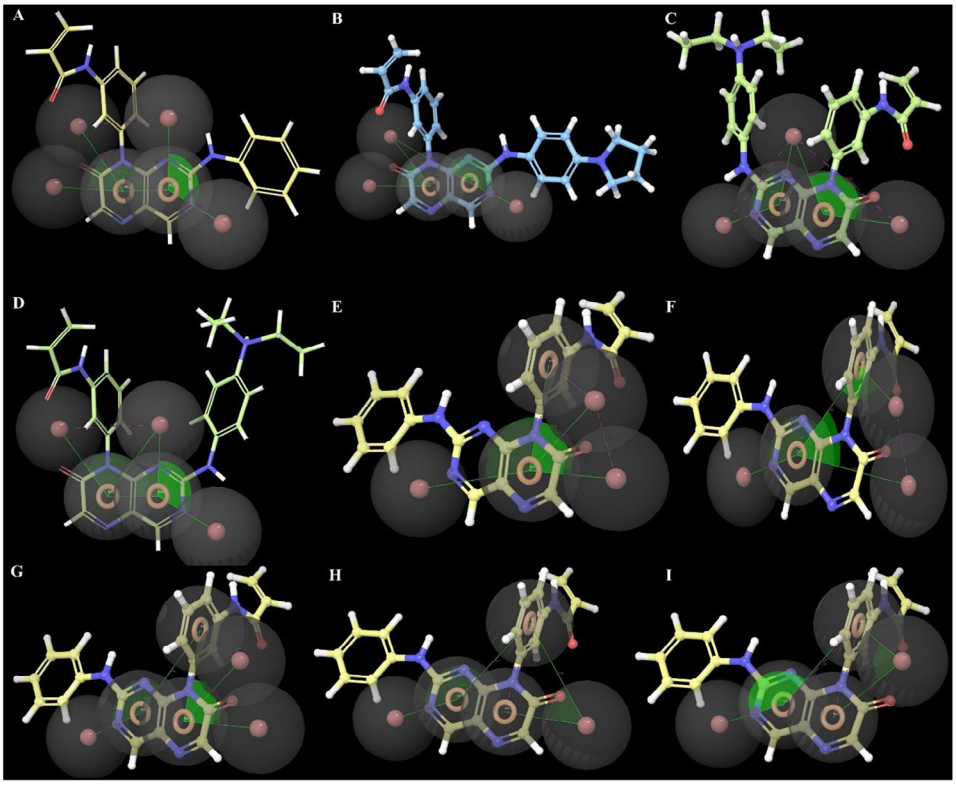

Figure 3. 3D representation of A) AAAARRR_2 (ZINC000096933693), B) AAARR_2 (ZINC000096933669), C) AAARR_4, D) AAARR_3 (ZINC000096933670), E) AAARR_4 (ZINC000096933670), F) AAARR_5 (ZINC000096933693), G) AAARRR_3 (ZINC000096933693), H) AARRR_1 (ZINC000096933693), and I) AARRR_2 (ZINC000096933693). *The green area is used to show the angle formed by the three features, and the light red dashed line is used to show the distance between the two features.

Table 4. Acylhydrazine-1-carbothioamide analogs (**4a–4l** and 11).

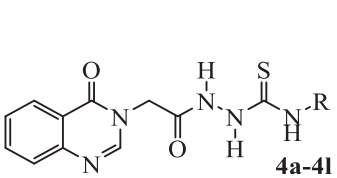

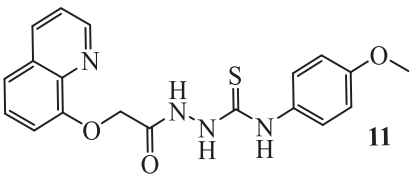

	R		R		R
4a	4-Methoxyphenyl	**4e**	3-Methylphenyl	**4i**	2-Chlorophenyl
4b	3-Methoxyphenyl	**4f**	2-Methylphenyl	**4j**	4-Fluorophenyl
4c	2-Methoxyphenyl	**4g**	4-Chlorophenyl	**4k**	Phenyl
4d	4-Methylphenyl	**4h**	3-Chlorophenyl	**4l**	Ethyl

compounds were obtained as stated in the literature[45] with C—F bond cleavage, and those were observed in the carbons to which fluoro was attached and the carbons adjacent to this carbon. The peaks of C═O and C═S structures were at 167.06–172.03 and 180.87–182.22 ppm, respectively. The peaks of the carbonyl carbon of the acetamide group of the molecules within series **8** and **13** were observed at 166.52–172.34 ppm. As a result, it was concluded that the observed ^{13}C-NMR data of the synthesized compounds were consistent with the expected values.

HRMS spectra also prove that the target compounds were successfully obtained. In addition, HPLC spectra for randomly selected compounds (**4h**, **8h**, **8s**, and **13a**) among each series were analyzed to prove the purity of the compounds.

2.3. Results and Discussion of Experimental Studies

2.3.1. Cytotoxicity Results

The cytotoxic effects of the compounds were calculated as IC_{50} (μM) based on the finding of 24 h in vitro studies. The results are shared in **Table 6**. The IC_{50} value of cisplatin was calculated to

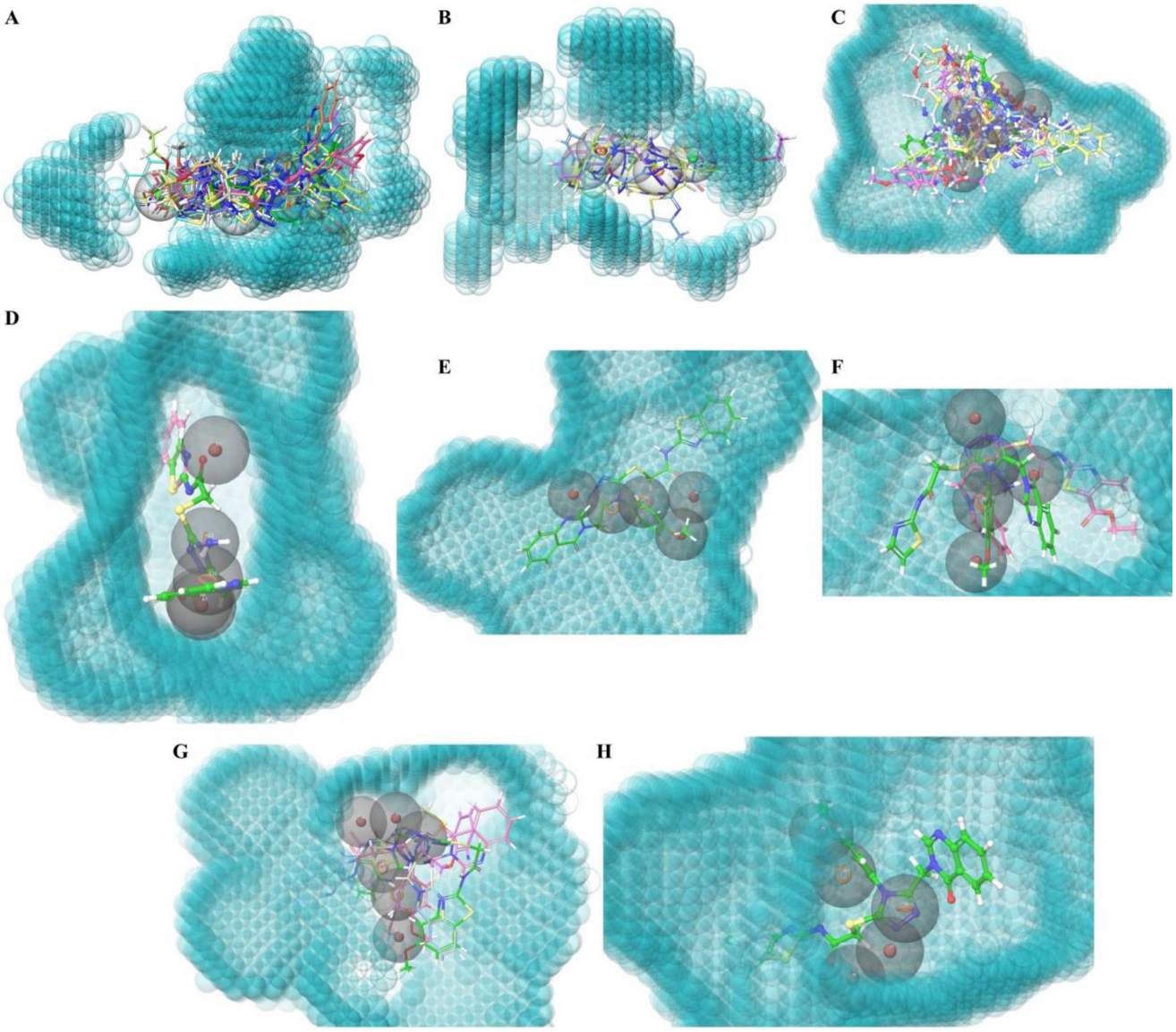

Figure 4. Hit molecules of the 3D superimposed from the hypotheses. A) DHHRRR_1, B) DHRRR_3, C) AAAARR_2, D) AAARR_5, E) AAARR_2, F) AAARR_3, G) AAARRR_3, and H) AAARR_6. Blue bubbles represent the excluded volume. For clarity, the external volumes on the front surface have been blurred.

be $27.33 \pm 6.81 \times 10^{-6}$ M. Thus, compounds that are either more active than cisplatin while do not show high cytotoxic effects on the healthy cells or even less active than cisplatin while do not show any cytotoxicity are **8d**, **4h**, **8b**, **4g**, **8l**, **8m**, **8e**, and **8o**, in descending order in terms of activity strength.

It is noteworthy that the most active derivatives of series **4** include *para*- (**4g**; $13.33 \pm 4.04 \times 10^{-6}$ M) and *meta*-chlorophenyl (**4h**; $4.90 \pm 0.66 \times 10^{-6}$ M) substitutions, whereas *ortho*-chlorophenyl substituent decreased cytotoxicity more than ten times. The highest activity among methoxyphenyl derivatives was found at the *ortho* position (**4c**; $86.67 \pm 7.64 \times 10^{-6}$ M), while the lowest activity was observed at the *para* position (**4a**; $201.00 \pm 3.61 \times 10^{-6}$ M). The opposite was observed for methylphenyl derivatives, with the highest activity at the *para* position (**4d**; $81.67 \pm 10.41 \times 10^{-6}$ M) and the lowest activity at the ortho (**4f**; $181.67 \pm 22.55 \times 10^{-6}$ M) position. The cytotoxic effect was reduced ten times when the chloro atom at the *para* position was substituted by the fluoro atom (**4j**; $136.67 \pm 41.93 \times 10^{-6}$ M). When hydrogen (**4k**; $186.67 \pm 12.58 \times 10^{-6}$ M) was substituted instead of fluoro, the cytotoxic efficiency was reduced even further. Finally, when the aromatic ring was replaced with the ethyl group (**4l**; $198.33 \pm 7.64 \times 10^{-6}$ M), the cytotoxicity decreased, but this effect was not as significant as others.

The cytotoxic effect of compound **5** ($>250 \times 10^{-6}$ M) that produced from compound **4a** was determined to be negligible. However, the anticancer activity of compounds **8a–8k**, which were synthesized from compound **5**, was shown to be highly cytotoxic (**8d**, IC_{50}: 3.63×10^{-6} M). These findings point out that the cyclization process has a negative effect on the cytotoxic activity; however, the combination with acetamide moiety increases again

Table 5. Triazole analogs of the pharmacophore molecules.

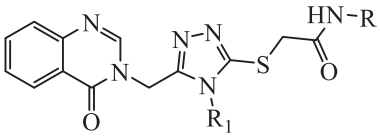

8a-8v

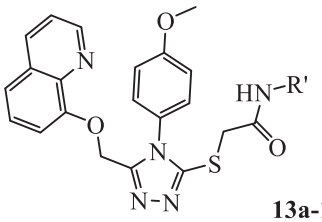

13a-13d

R_1*	R_1**	R		R'
8a	**8l**	6-Fluorobenzothiazol-2-yl	**13a**	Thiazol-2-yl
8b	**8m**	6-Chlorobenzothiazol-2-yl	**13b**	4-Methyl-5-acetyl-thiazol-2-yl
8c	**8n**	6-Nitrobenzothiazol-2-yl	**13c**	4-Methyl-5-(ethoxy carbonyl)-thiazol-2-yl
8d	**8o**	Benzothiazol-2-yl	**13d**	4-(Ethoxy acetyl)thiazol-2-yl
8e	**8p**	6-Methylbenzothiazol-2-yl		
8f	**8q**	6-Methoxybenzothiazol-2-yl		
8g	**8r**	6-Ethoxybenzothiazol-2-yl		
8h	**8s**	Thiazol-2-yl		
8i	**8t**	4-Methyl-5-acetylthiazol-2-yl		
8j	**8u**	4-Methyl-5-(ethoxy carbonyl)-thiazol-2-yl		
8k	**8v**	4-(Ethoxy acetyl)thiazol-2-yl		

Note: R_1* for **8a–8k** is 4-methoxyphenyl, and R_1** for **8l–8v** is amino group.

the cytotoxicity. It is supposed that the effect was decreased due to steric factors such as the restriction of access to heteroatoms in the structure due to cyclization. In addition, the closure of the ring along with the aromaticity increased the hydrophobic effect and produced a decrease in the structure's polarity, indicating that physicochemical features play a role in the cytotoxicity of these analogs. Besides that, the presence of free heteroatoms in the molecules seems to be responsible for of the increased cytotoxicity caused by the acetamide moiety. Among analogs of **8a–8k**, the most cytotoxic derivatives contain benzothiazole (**8d**; $3.63 \pm 0.81 \times 10^{-6}$ M), 6-chlorobenzothiazole (**8b**; $12.50 \pm 0.71 \times 10^{-6}$ M), and 6-methylbenzothiazole (**8e**; $23.67 \pm 6.66 \times 10^{-6}$ M), respectively. Generally, benzothiazole derivatives are more effective than thiazole derivatives (**8h–8k**). In fact, nonsubstituted thiazole (**8h**); 4-methyl-5-acetyl thiazole (**8i**), and 4-ethoxyacetylthiazole (**8k**) did not show any cytotoxicity, while 4-methyl-5-ethoxycarbonylthiazole (**8j**; $103.33 \pm 2.89 \times 10^{-6}$ M) showed inhibitory effect against A549 cells. The remarkable point here is that the cytotoxic activity of compound (**8j**) decreased when the molecule was elongated by one carbon atom **(8k)** or lost acidity **(8i)**.

Compound **7** was not cytotoxic on A549 cells, similarly, its analog, compound **5**. However, the cytotoxic activity of **8l–8v**, derived from compound **7**, is significantly increased. The substitution effects on quinazolin-4(*3H*)-one can be explained by the decrease in the acidity of the side chain when considering compounds **4a**, **5**, **7**, and **8a–8v**. However, the low anticancer effect of some derivatives which include ester groups (**8j**, **8k**, **8u**, and **8v**) point out that the increase in acidity of molecule is not effective beyond a certain level.

Among the **8l–8v** analogs, the most active derivatives are 6-fluorobenzothiazole (**8l**; $13.75 \pm 1.77 \times 10^{-6}$ M), 6-chlorobenzothiazole (**8m**; $21.50 \pm 0.71 \times 10^{-6}$ M), and benzothiazole (**8o**; $38.50 \pm 12.02 \times 10^{-6}$ M), respectively. In fact, benzothiazole derivatives (**8l–8r**) are more active than thiazole derivatives (**8s–8v**). Similar to *N*-(4-methoxyphenyl)triazole analogs, the compound contains 4-methyl-5-ethoxycarbonylthiazole (**8u**, $98.33 \pm 5.77 \times 10^{-6}$ M) is the only derivative that shows cytotoxicity against A549 cell line among thiazoles.

Using *N*-(4-methoxyphenyl)triazole pattern, compound **12** which includes a quinoline ring was also obtained, and this structure was substituted with thiazol-2-ylacetamide derivatives (**13a–13d**). When the quinazoline starting compound (**5**) and quinoline starting compound (**12**, $178.33 \pm 42.53 \times 10^{-6}$ M) were compared, quinoline was more cytotoxic against A549 cells than its quinazoline analogue. On the other hand, 4,5-nonsubstituted- (**13a**), and 5-acetyl-4-methyl (**13b**) thiazoles, which were obtained using compound **12**, showed anticancer activity. Moreover, these two compounds were 2.65 and 2.33 times more active than compound **12**, respectively. In contrast to that, ethyl ester analogs of quinolines (**13c** and **13d**) did not show any cytotoxic effect. Like their quinazoline analogs, the difference in activity is clearly related to the decreasing acidity of the structure, which has a negative impact on their activity.

2.3.2. Apoptotic Effects

Annexin quadrants and their percentages are given in **Figure 5** and **Table 7**. While the sum of the early and late apoptotic effects of cisplatin was calculated as 22.61%. The total apoptotic percentages of compounds **4g**, **4h**, **8b**, **8d**, **8e**, **8l**, **8m**, and **8o** were 31.08, 15.66, 77.68, 8.59, 6.66, 23.95, 15.17, and 14.03, respectively. Briefly, compound **8b** showed the highest apoptotic effect, and had ≈3.5 times higher apoptotic effect than cisplatin, while

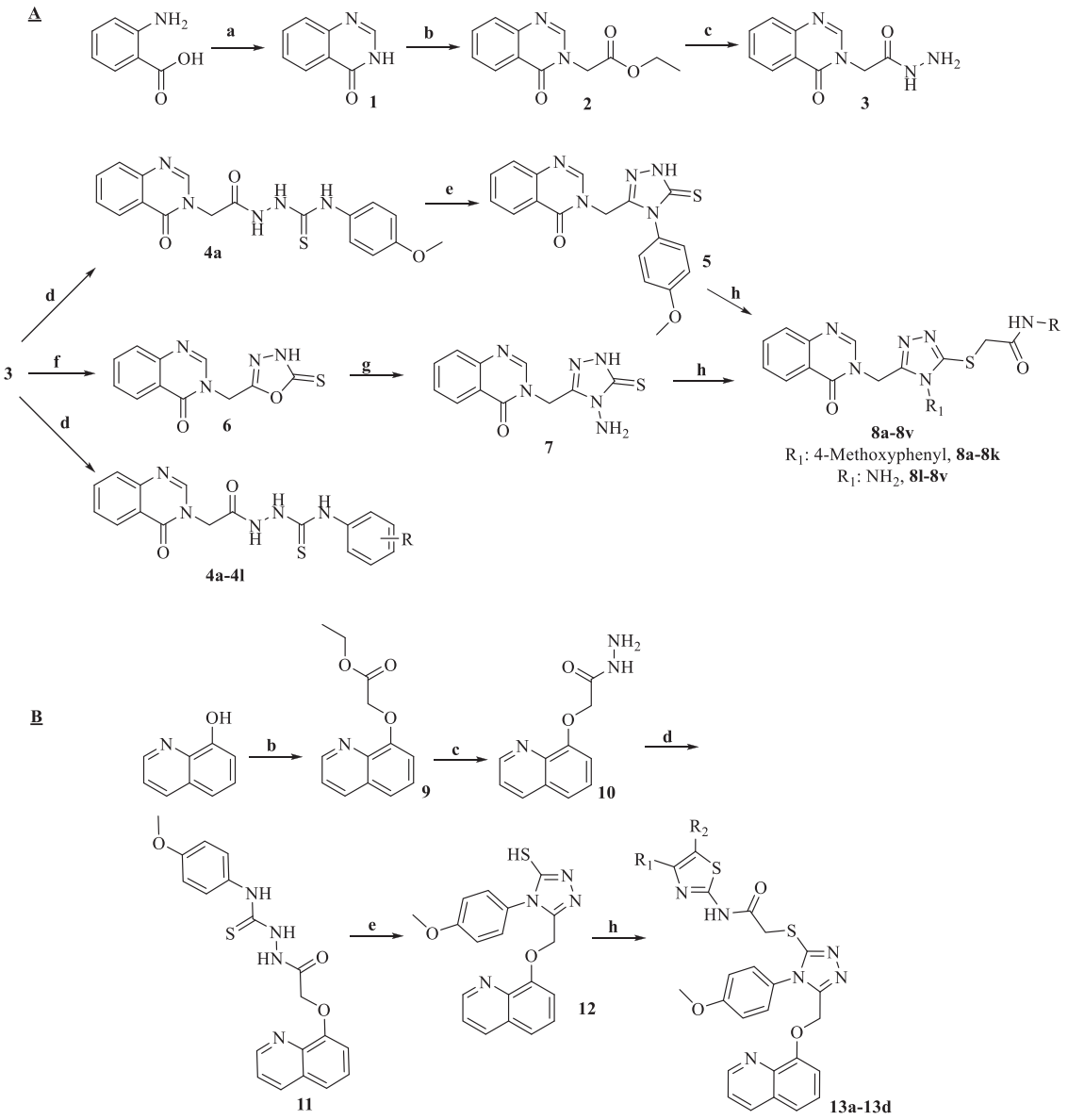

Scheme 1. Synthesis of the hit molecules and their analogs. A) Synthesis route of quinazoline derivatives, and B) synthesis route of quinoline derivatives. *Reaction conditions*: a) $HCONH_2$, oil bath/6 h or MW/15 min. b) $BrCH_2COOEt$, Acetone, K_2CO_3, reflux. c) $N_2H_4{\cdot}H_2O$, rt overnight. d) R-NCS, dropping at 0 °C, then stir at rt. e) EtONa at 0 °C, then reflux 2 h. f) CS_2, EtONa, 0 °C, then reflux 2 h. g) $N_2H_4{\cdot}H_2O$, reflux 2 h. h) Aryl acetamide derivatives, K_2CO_3, acetone, rt.

compounds **4g** and **8l** induced apoptosis with a similar profile to cisplatin.

2.3.3. Determination of the Mechanism of Action

After determining the apoptotic activity, the apoptosis-inducing effect was investigated. Apoptosis, which is type-1 programmed cell death, is known to occur through the activation of two main pathways, the intrinsic pathway and the extrinsic pathway. The intrinsic pathway, also referred to as the mitochondrial pathway, initiates a cascade of events triggered by a death signal caused by the mitochondria's inability to produce ATP through glycolysis. This leads to the release of Cytochrome C and the formation of the apoptosome, which combines with caspase-9 to form a new complex. This complex subsequently activates the effector caspase, caspase-3. On the other hand, the extrinsic pathway involves the activation of caspase-8 through death receptors present on the cell membrane surface, which also activates caspase-3. The activation of caspase-3 plays a crucial role in both the intrinsic and extrinsic pathways, serving as a convergence point for inducing apoptosis.[46]

Caspase-3 Results: The caspase-3 activation results and their quadrants are given in **Table 8** and **Figure 6**, respectively.

The induction of caspase-3 by cisplatin was calculated to be 34.39%. The compounds were then ranked from the most to the

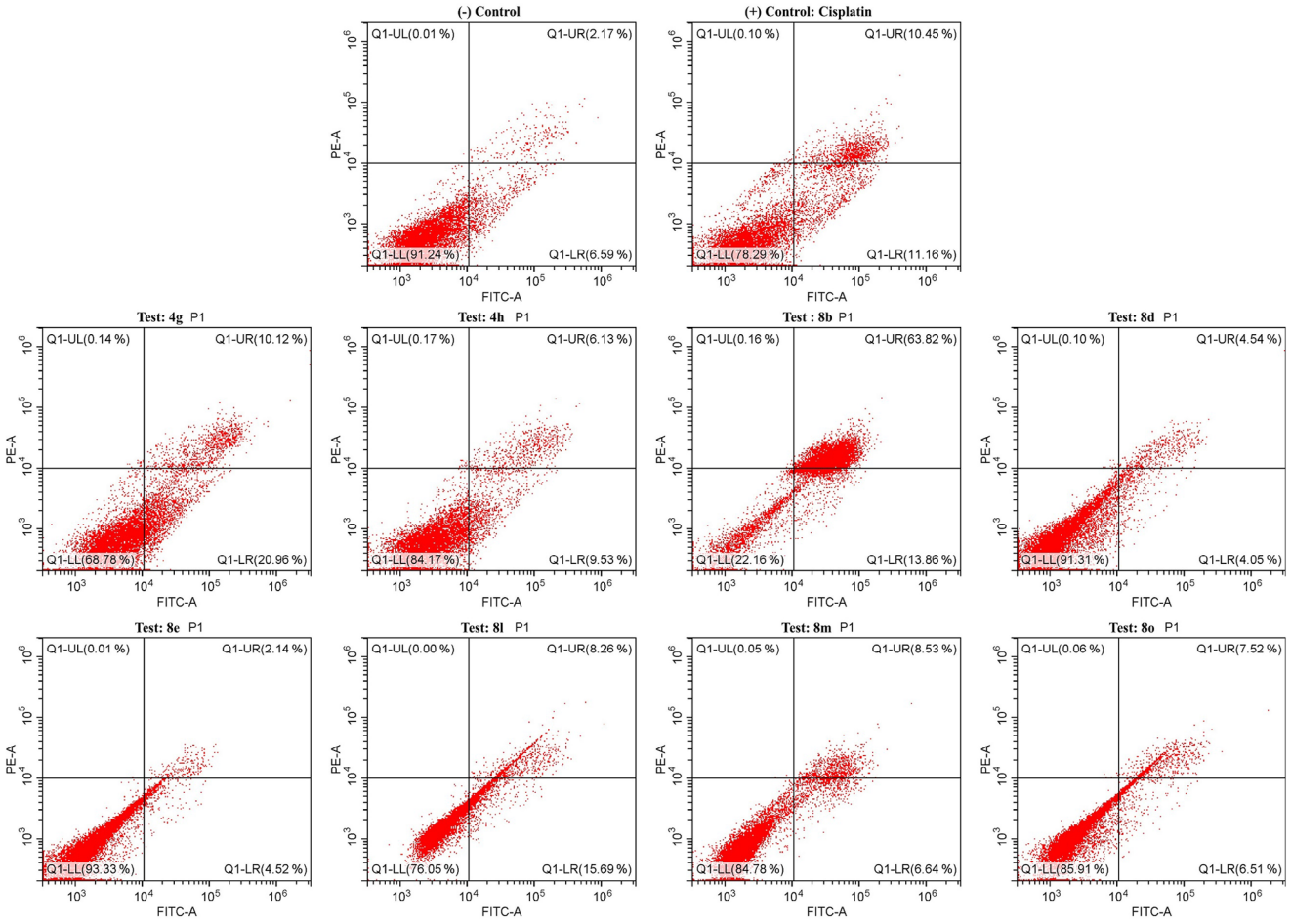

Figure 5. Annexin quadrants* of active compounds and standard drugs. *No active substance was used in the negative control. Cisplatin was used as a positive control. Compounds with high anticancer activity and selectivity index were marked as active compounds. Each experiment was replicated for four times, and at least 10^4 cells per sample were analyzed, and quadrant analysis was performed.

least effective as follows: **8l**, **8b**, **8m**, **8o**, **8e**, **8d**, **4g**, and **4h**. In fact, the induction values of **4g**, **4h**, **8d**, and **8e** were found to be less effective compared to cisplatin. On the contrary, the activities of compounds **8l**, **8b**, and **8m** were found to be more active than cisplatin's activity. In conclusion, compounds containing halogen atoms, specifically chloro (**8b** and **8m**), and fluoro (**8l**), exhibited greater effectiveness. Based on this result, it can be suggested that caspase-3 activation rises as lipophilicity increases.

Mitochondrial Membrane Depolarization: **Figure 7** displays the plots representing the results of the mitochondrial membrane depolarization test while **Table 9** provides the corresponding percentage values. The mitochondrial membrane depolarization value of cisplatin was 36.01%, while the values of **4g** (15.41%), **4h** (14.48%), and **8e** (28.96%) were lower than cisplatin. On the other hand, compound **8b** (75.30%) is 2.09 times, compound **8d** (61.62%) is 1.71 times, compound **8l** (96.13%) is 2.67 times, compound **8m** (83.70%) is 2.32 times, and compound **8o** (75.30%) is 2.09 times more than cisplatin. Basically, it caused mitochondrial dysfunction by inducing depolarization. Although there are various mechanisms that can cause mitochondrial membrane depolarization,[47] as mentioned in a previous mechanistic study,[48] it predominantly occurs in non-small cell lung cancer cells. Indeed, the fact that the design of compounds was based on EGFR inhibition, and the observation of such results highlighted the necessity to elucidate EGFR enzyme mechanics both computationally and experimentally.

Evaluation of EGFR Inhibition: The IC_{50} values of EGFR inhibition are presented in **Table 10**. The IC_{50} value of gefitinib (positive control) was determined as $4.169 \pm 0.156 \times 10^{-9}$ M. The most active ones were **4h** ($5.298 \pm 0.164 \times 10^{-9}$ M), **8d** ($5.46 \pm 0.221 \times 10^{-9}$ M), **8l** ($2.670 \pm 0.124 \times 10^{-9}$ M), and **8m** ($2.191 \pm 0.908 \times 10^{-9}$ M). These compounds share two common features. First, they contain a quinazolin-4(*3H*)-one moiety. Second, they possess halogen-substituted aromatic structures, except for compound **8d**.

2.4. Results of In Silico Studies

2.4.1. Evaluation of Molecular Docking and Dynamics Simulation of Active Compounds-Caspase-3 Protein

The docking studies are displayed in **Figure 8**, and the interactions are shared in **Table 11**. In a previous study,[49] Arg64,

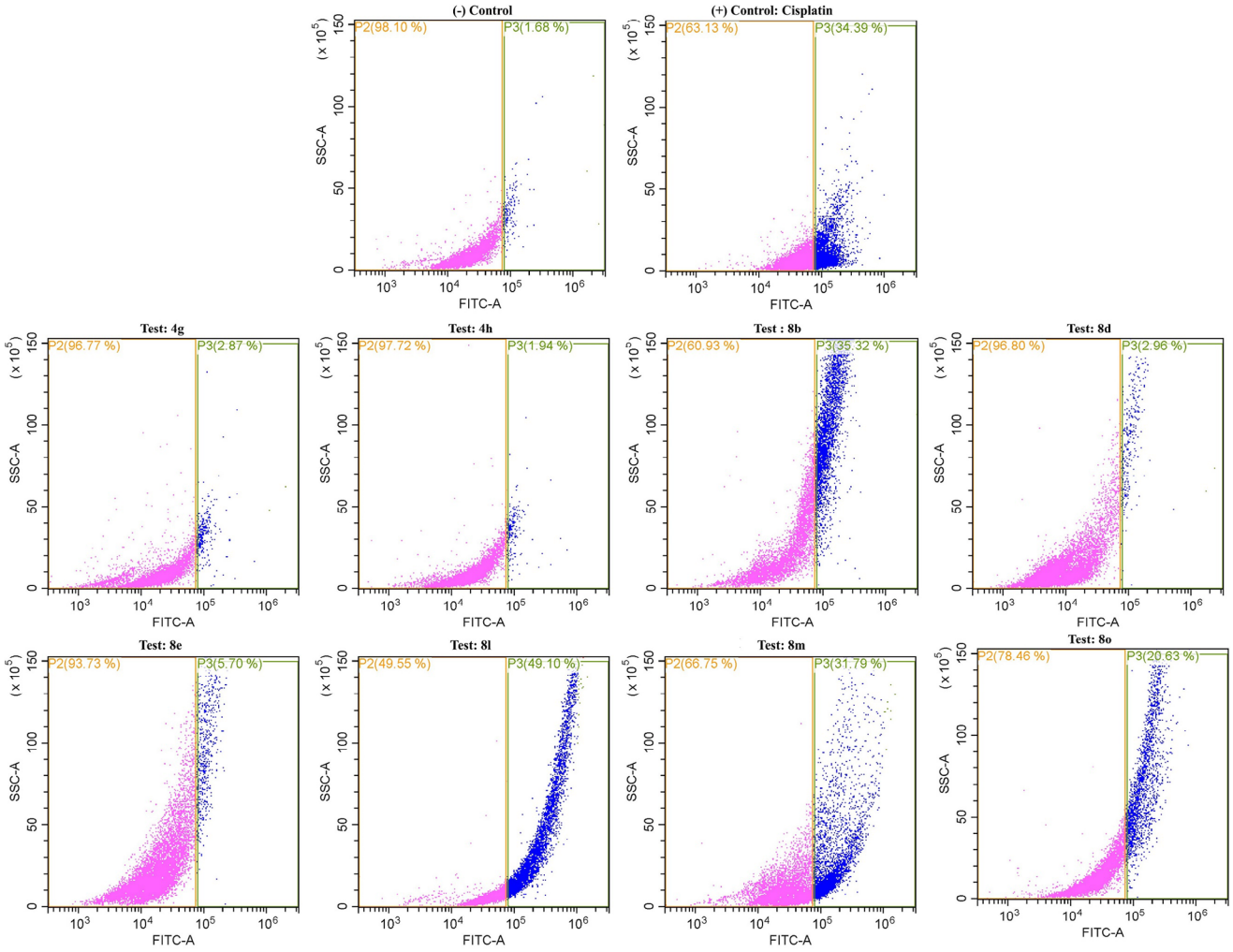

Figure 6. Results of active compounds and standard drugs. *No active substance was used in the negative control. Cisplatin was used as a positive control. Compounds with high anticancer activity and selectivity index were marked as active compounds. Each experiment was replicated for four times, and at least 10^4 cells per sample were analyzed, and quadrant analysis was performed.

Ser120, His121, Gly122, Gln161, Cys163, Tyr204, Ser205, Trp206, Arg207, Asn208, Ser209, Ser249, and Phe250 amino acids were identified as binding region residues.

According to the obtained results, 4-amino-1,2,4-triazole analogs (**8l**, **8m**, and **8o**) interacted with Arg64 (Asn52-Gly66 loop), Hie121, Gly122 (ß-strand: Hie121-Glu123), Tyr204, Arg207 (Ser198-Ser213 loop), and Phe256 (Phe247-Pro263 loop) and exhibited similar types of interactions with these residues. Interestingly, among the *N*-(4-methoxyphenyl)triazole analogs, only **8b** demonstrated an interaction with Arg207. It is proposed that the main reason for this discrepancy is the orientation of the bulky 4-methoxyphenyl group to the Phe250 amino acid as compound **8b** was far away from Arg64, leading to the loss of the interaction compared to its analogs. In contrast, while 4-amino-1,2,4-triazole derivatives can form one or two hydrogen bonds with Arg207, compound **8b** exhibited additional interactions including ionic, hydrophobic, and aromatic hydrogen bonds. Furthermore, compound **8b** forms aromatic H-bonds with Ser120, Trp206, and Trp214 residues. Compounds **8m** and **8o** form H-bond with Glu123 and Ser205. It was determined that **8l** interacts with Gln161 (ß-strand: Leu157-Gln161) and Cys163. Considering all these interactions within the binding site, and despite the slight variation in the localization of compound **8b**, it is proposed that it exhibits the similar activation effect due to its interaction with the same loop residues. Furthermore, all four compounds form bonds with nearby residues outside the binding site, especially with various loop amino acids. These interactions contribute to the stabilization of the ligand–protein complex, ultimately imparting rigidity to the enzyme structure. In conclusion, this docking study has confirmed that all four compounds have strong interactions with the Ser198–Ser213 loop region, which is reported to have a key role in caspase-3 allosteric activation. Since the acetamide structures of compounds interact with these loop amino acids, it can be defined as a pharmacophore core.

Unlike the other three analogs, compound **8l** exhibits higher activity due to the formation of a salt bridge in addition to H-bonds with Arg64 and Gln161, as it was hypothesized. Moreover, 4-amino-1,2,4-triazole derivatives have an amine group instead

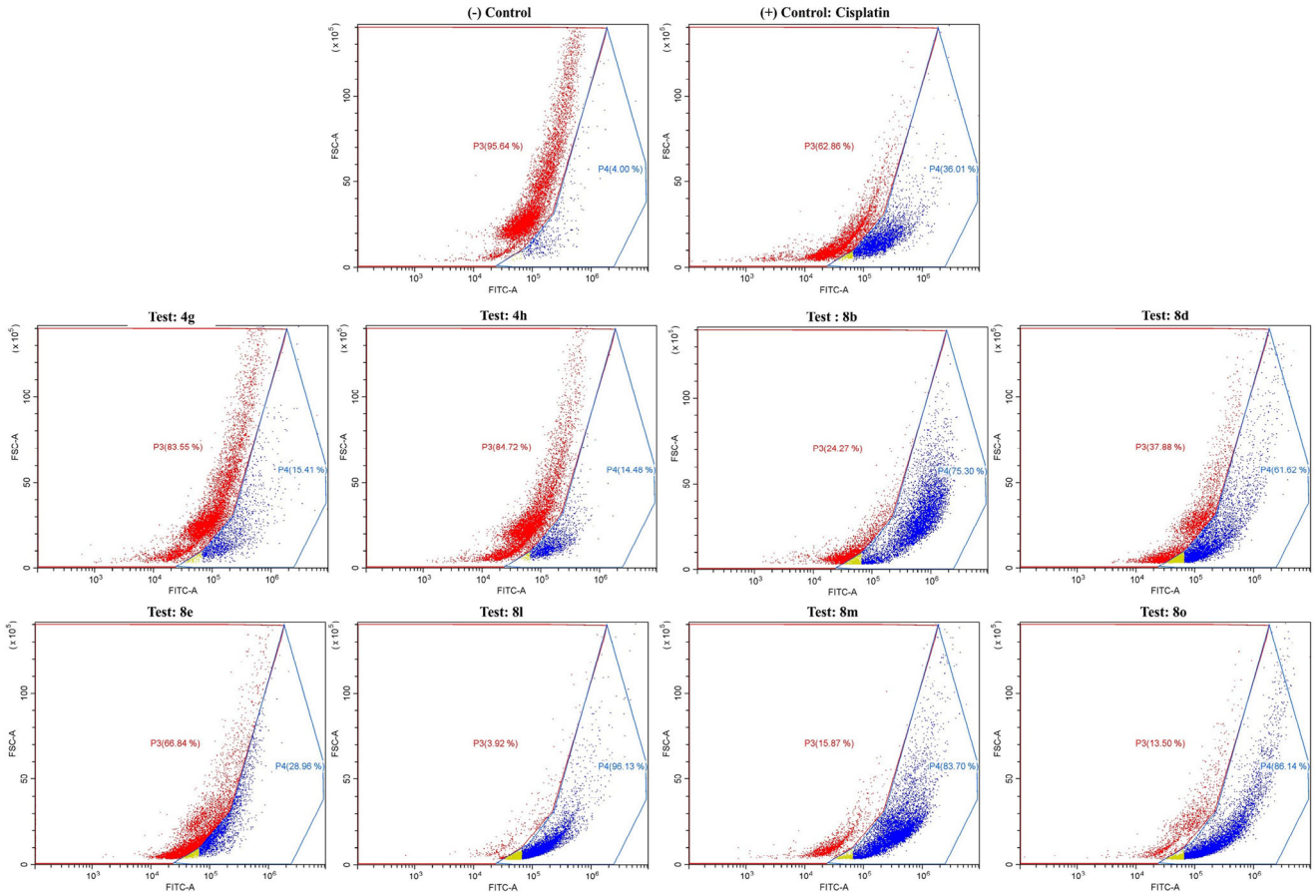

Figure 7. Quadrants of mitochondrial membrane polarization and depolarization of active and standard compounds. *Mitochondrial membrane polarization and depolarization was determined using A549 cells.

of a phenyl, which enhance the molecule's rotability, enabling it to adapt into the gap between Arg64 and Arg207. The stability of this gab is based on the formation of H-bonds with these residues (Figure 8C).

As a result, the experimental results of the compounds are consistent with the docking study, providing an explanation for the binding mode and structure–activity relationship on the caspase-3 enzyme. In addition, MDS study was conducted by using compound **8l** as a reference, this study aimed to investigate the effects of time and environmental changes, such as the presence of water and various ions, on the compound. MDS results are presented in **Figure 9**, where panels (A) to (C) display the stability values of the complex, and panels (D) to (F) demonstrate the interactions. As descripted in previous studies,[50,51] the stability plots showed that the RMSD values remain within the range of 1–3 Å after 0.2 ns, with a maximum peak observed at 2.64 Å at around 7.60 ns. Furthermore, the Rg values exhibit minimal fluctuation, and the peaks of rigid regions were calculated between 0.36 and 0.93 Å. So, it can be concluded that the stability of the complex was maintained throughout the entire simulation time.

According to Video S1 (Supporting Information) and Figure 9D–F, the interaction analysis revealed the presence of various types of interactions between compound **8l** and the caspase-3 enzyme. These interactions included conventional hydrogen bonds, water-mediated hydrogen bonds, hydrophobic interactions (such as π–π stacking and π–cation interactions), and an ionic interaction (salt bridge). Conventional hydrogen bonds were observed with Arg64, Gln161, Cys163, Ser205, Trp206, and Arg207 while water-mediated H-bonds were with Thr62, Arg64, Ser120, His121, Gln161, Tyr204, Ser205, Trp206, Arg207, Asn208, Ser249, Phe250, Ser120, and Phe251. Hydrophobic interactions were observed with Met61, His121, Tyr204, Trp206, and Phe256 residues. Finally, the salt bridge was formed only with Arg64. Among all these interactions, the most significant ones were with Arg64, Cys163, Ser205, and Arg207 due to their consistent presence. However, in terms of interaction strengths, the following order was observed; H-bond between Arg207 and acetamide oxygen (143%), H-bond between Cys163 and benzimidazole nitrogen (99%), H-bond between Ser205 and hydrogen of 4-amino-1,2,4-triazole nitrogen (99%), water-mediated H-bond between Arg64 and acetamide nitrogen (69%), H-bond between Trp206 and quinazoline nitrogen (N_1) (63%), water-mediated H-bond between Ser120 and acetamide nitrogen (61%), Arg207 and hydrogen of 4-amino-1,2,4-triazole nitrogen (53%), salt bridge between Arg64 and acetamide nitrogen (50%), water-mediated H-bond between Arg64 and acetamide nitrogen (42%), π–π stacking between Phe256 and

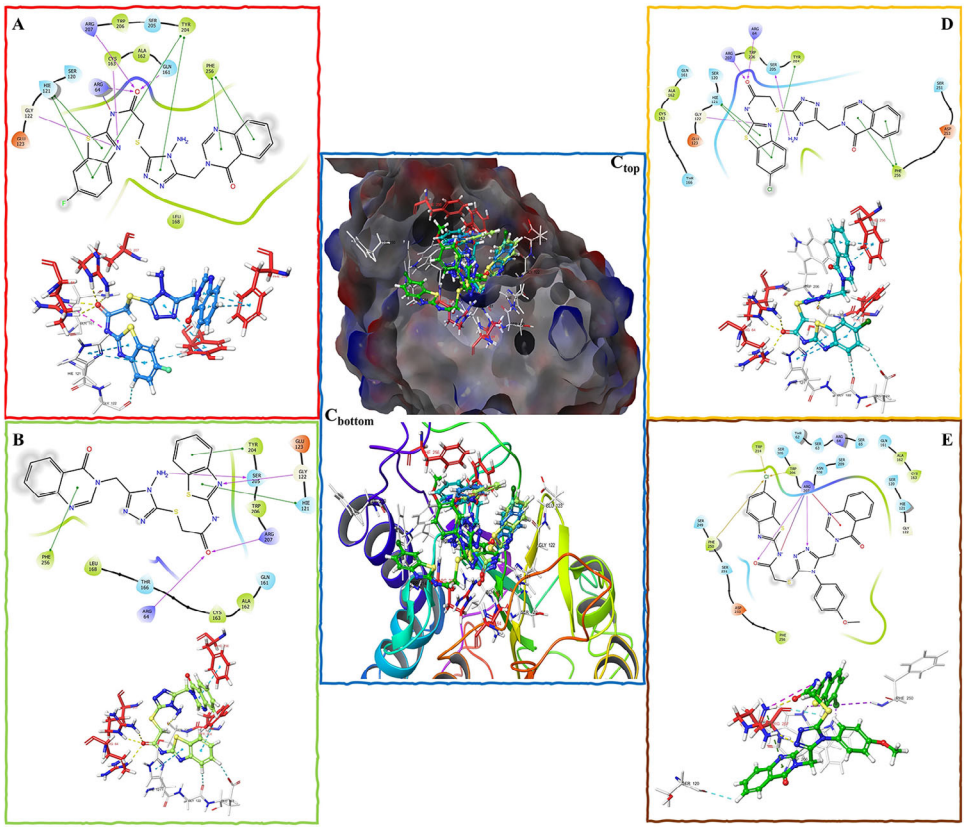

Figure 8. 2D- and 3D-docking poses of active compounds on caspase-3 (PDBID: 4QTX). Box A: **8l**; Box B: **8m**; Box C: Superimposed of all actives; C_{top}: Surface area of enzyme colored by electrostatic properties; C_{bottom}: Enzyme quaternary structure; Box D: **8o; Box E: 8b**.

the quinazoline ring (42%), π–π stacking between His121 and benzothiazole ring (40%), π–π stacking between Tyr204 and the quinazoline ring (36%), and water-mediated H-bond (20%) between Arg207 and the triazole nitrogen (N_4). Based on above findings, the following statements are suggested:

- H-bonds with 204–209 loop region were formed with acetamide residue, thus it is an important caspase-3 pharmacophore structure.
- The incorporation of pharmacophore structure, acetamide, along with a nonbulky triazole and a benzothiazole moiety, which enhance the lipophilicity, has a beneficial impact on the allosteric effect mediated by His121, Gln161, Cys163, Trp206, and Arg207.
- Finally, the exposure of the quinazolin-4(3H)-one moiety to the solvent environment promotes stability, and its π-π stacking with Phe256 contributes to this stabilization effect while benzothiazole ring plays a significant role in inducing caspase through continuous H-bond formation with Cys163.

Based on the information provided, one of the potential structural modifications for caspase-3 activation is the changes on the quinazolin-4(*3H*)-one structure that can interact with the solvent. one suggestion is to introduce acylation at the sixth and seventh positions. Another one is to incorporate polar but non-aromatic structures that can serve as hydrogen bond acceptors with straight heteroatom chains (such as ether group). On the other hand, the 4-amino-1,2,4-triazole structure should be unchanged as it is considered an optimum structure for the desired activity. Regarding the modifications in the benzothiazole ring, it is recommended to prioritize solubility properties rather than focusing solely on binding interactions with amino acids. This ensures that the modified compounds have favorable solubility characteristics, which can contribute to their overall effectiveness.

2.4.2. Evaluation of Molecular Docking and Dynamics Simulation of Active Compounds-EGFR Protein

In **Figure 10** and **Table 12**, the results of molecular docking study were presented for active compounds that exhibited potency under 10×10^{-9} M in experimental studies.

According to the literature,[52] the hinge region (seq. 791–796) has been identified such as intersection between N and C tail, hence, it plays a major role in the inhibitory activity. EGFR inhibitors, such as gefitinib located in this region, and form a hydrogen bond with the backbone nitrogen of Met793. Typically, there is one hydrogen bond formed. In addition, the hydrophobic side pocket, known as the ATP binding site, is surrounded by the side chain of amino acids such as Lys745, Leu788, and Thr790, and it has been observed that the hydrophobic parts of EGFR inhibitors, such as aniline-based compounds, can fit into this pocket.

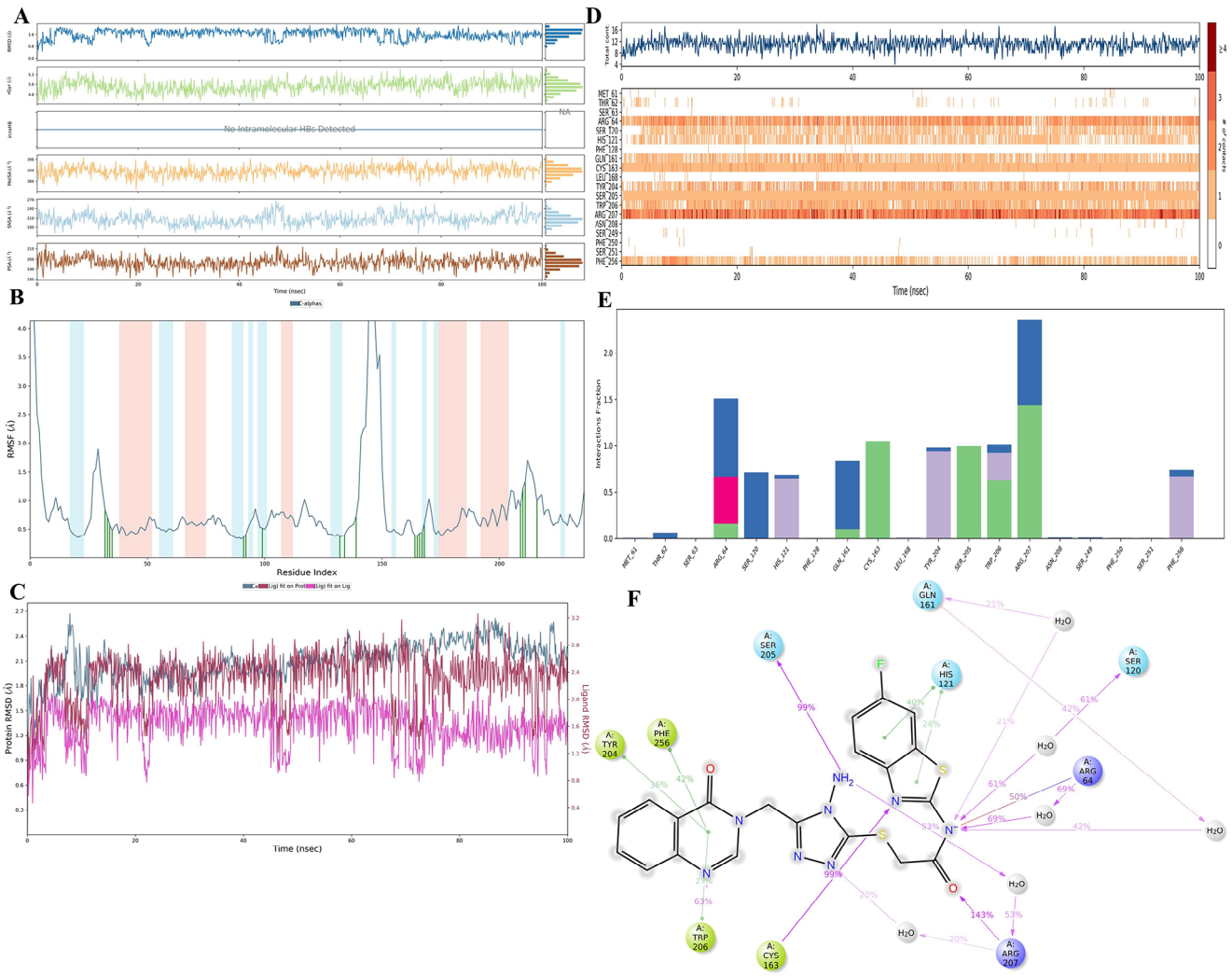

Figure 9. MDS plots of **8l**-Caspase-3 complex. A) Changes of physicochemical parameters (RMSD, Rg, intra-H bond, MolSA, SASA ve PSA) of **8l** during simulation time; B) plot of RMSF–amino acid indexing; C) RMSD–time plot; D) plot of total interaction–amino acid fraction versus time; E) histogram of interaction type and interaction fraction; and F) bond strengths (cutoff = 20%).

In this study, it was found that the active compounds exhibit common interactions with Lys745, Arg841, and Asp855. Furthermore, these compounds show similar binding patterns with the hinge amino acids Gln791 and Met793, except for compound **8d**. Due to the side chain, 4-(4-methoxyphenyl)triazole of compound **8d** exhibits a different orientation in the ATP region. As a result, the quinazolin-4(*3H*)-one moiety of compound **8d** could not approach the Met793 amino acid at the right angle, leading to the formation of a H-bond only with Cys797, which is also the hinge region amino acids. In addition, it was observed that only compound **4h** interacts with Thr854, while compound **8m** forms aromatic H-bond specifically with the amino acid Ser720, which is a member of the phosphate binding (P loop) domain.

It was found that the two most active compounds (**8l** and **8m**) exhibit very similar binding positions. Although there was a slight shift because of fluoro/chloro difference, they display comparable interactions in the ATP-binding region and hinge region. This localization is similar to the positioning of the side chain observed in EGFR-TK inhibitors, -tinibs (such as the morpholinopropoxy group in gefitinib). Basically, these compounds extend outward from the receptor, allowing for the interaction with the solvent region.

In conclusion, EGFR inhibition leads to mitochondrial membrane depolarization and activation of caspase-3 pathway, which is particularly significant in the case of non-small cell lung cancer metastasis cases.[48] All in vitro and in silico studies conducted for mechanistic purposes up to now are in harmony and the behavior of compounds against proteins at the molecular level has been explained also by in silico studies. In addition to all these, considering the IC_{50} and apoptosis inductions obtained with the MTT results, compound **8l** was identified as the most potent compound. Therefore, to further understand the structure–activity relationship, molecular dynamics simulation was performed by modeling compound **8l**.

The MDS results are shown in **Figure 11** for the compound **8l**–EGFR complex. When the stability indicators of this complex (Figure 11A–C) are examined, the Rg, RMSD, and RMSF values are appropriate as stated in Section 2.4.1. This indicates that the

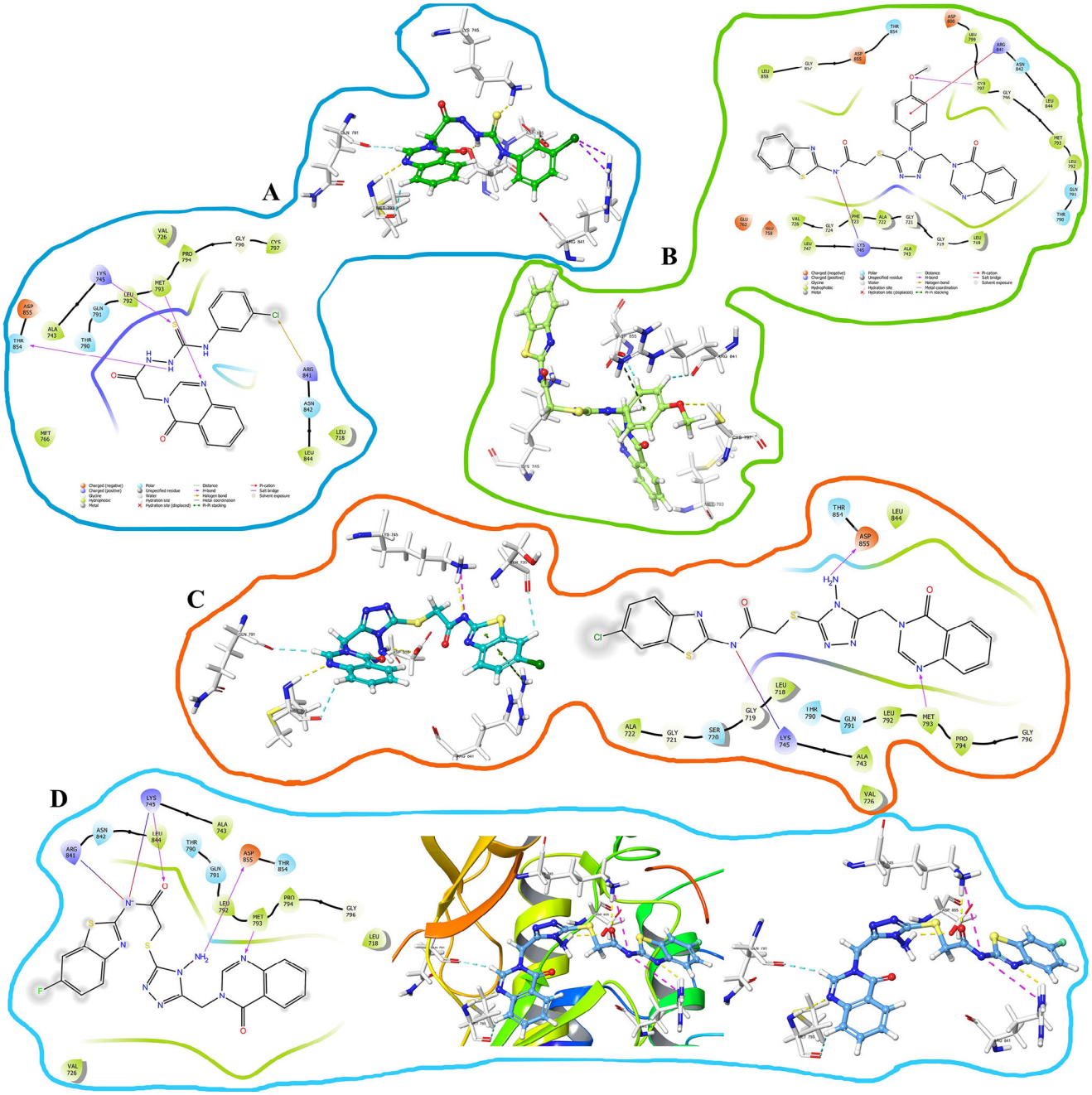

Figure 10. 2D- and 3D-docking poses on EGFR protein (PDBID: 2ITY). A) **4h**, B) **8d**, C) **8m**, and D) **8l**. The curves used for separating the compounds did not represent active pocket of the protein.

complex remains stable throughout the simulation period. Examining Video S2 (Supporting Information) and the graphs in Figure 11D–F, the most stable interactions were direct H-bonds with Lys745, Met793, Thr854, and Asp855, water-mediated H-bonds with Lys745 and Thr790, and π–cation interaction with Arg841. Although there is a temporary disruption in the interaction with Lys745 between 55 and 60 ns, after 60 ns.

Consistent with the results of molecular docking, the positioning of the **8l**–EGFR system is similar to the EGFR inhibitor drugs. The stability of the complex was supported by environmental factors and even an increase in the strength through water-mediated interaction. Occasionally, intramolecular hydrogen bonding has been observed between the oxygen of quinazolin-4(*3H*)-one and the hydrogen of the *N*-amine group of the triazole. Although the frequency of this interaction is low, it is suggested to be crucial for these two rings to keep their relative positions with respect to the protein.

H-bonding with Lys745 (ATP binding site) is considered to play a significant role in the activity of the compound. This interaction is observed via water-mediated H-bond, direct H-bond, and

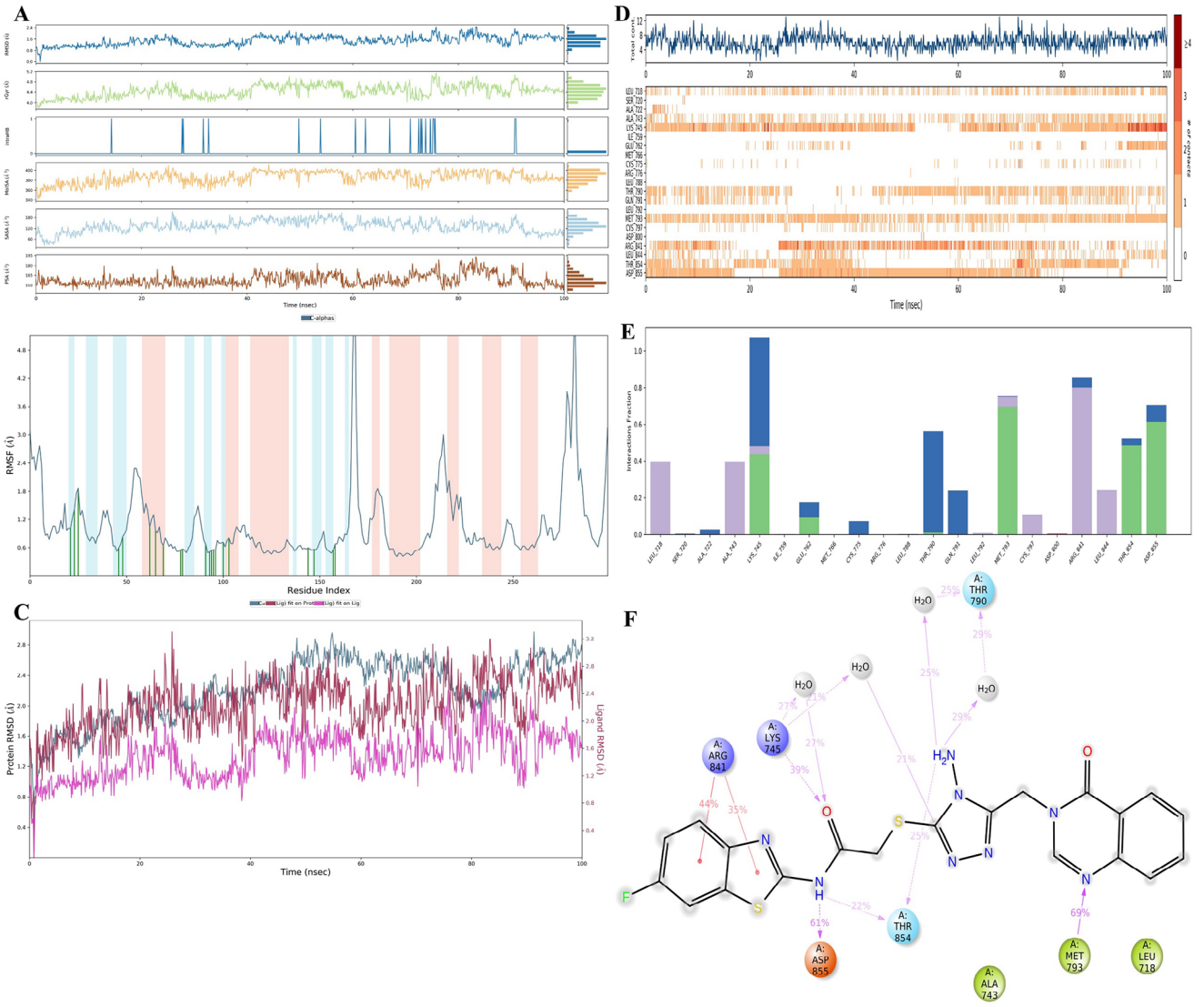

Figure 11. MDS results of compound 8l-EGFR complex. A) Changes of physicochemical parameters (RMSD, Rg, intra-H bond, MolSA, SASA ve PSA) of **8l** during simulation time; B) plot of RMSF–amino acid indexing; C) RMSD–time plot; D) plot of total interaction–amino acid fraction versus time; E) histogram of interaction type and interaction fraction; and F) bond strengths (cutoff = 20%).

hydrophobic interactions. Like the findings in the docking study, it is an evident that the quinazoline ring and benzothiazole ring located well and kept their position at the hinge region (Gln791 and Met793) and ATP binding site (Lys745). In addition to that, these findings suggest that the acetamide group also supports inhibition activity allosterically via interactions between Asp855 (allosteric region residue, the entrance of the ATP binding cleft) and nitrogen of acetamide. Based on our docking study and observations, the presence of halogen atoms in the benzothiazole moiety of the compounds contributes to their inhibitor activity since the benzothiazole is exposed to solvent exposure, but it also helped to moderate the stability of the complex by interacting with organic (such as phospholipids) and inorganic substances (such as water, sodium, chloro, etc., electrolytes) in the solvent environment. In line with this, structural modifications that involve replacing the halogen atom, such as fluor atom, with long-chain polar structures (e.g., morpholinopropyloxy as in gefitinib), have potential to increase inhibitor activity. These modifications can further optimize the interactions with the solvent environment, potentially leading to enhanced potency and efficacy of the inhibitor.

When the analogs of compound **4** were examined, it has found that the aromatic structures linked to the polar chain were effective when they have a hydrogen or halogen atom. Moreover, optimum activity was obtained with chloro substitution. In fact, the presence of chloro in the meta position of the phenyl ring has a higher anticancer and EGFR inhibition effect than the *para* position. When the analogs of **8** were examined, it was observed that an azole ring with at least two nitrogen atoms in the center without steric hindrance is essential. Also, an aromatic ring bonded with sp^3 atoms from the opposite positions of this central ring increases anticancer activity. Besides that, the bicyclic aromatic ring attached to the sp^3 carbon atom should be a quinazoline ring.

Table 6. Cytotoxicity results as IC_{50} (μM) against healthy and cancer cells.

Compound	A549	SD	L929	SD	SI
4a	201.00	3.61	>250.00	–	>1.24
4b	126.67	2.89	>250.00	–	>1.97
4c	86.67	7.64	>250.00	–	>2.89
4d	81.67	10.41	>250.00	–	>3.06
4e	88.33	7.64	>250.00	–	>2.83
4f	181.67	22.55	>250.00	–	>1.38
4g	13.33	4.04	>250.00	–	>18.76
4h	4.90	0.66	>250.00	–	>51.02
4i	133.33	32.16	>250.00	–	>1.88
4j	136.67	41.93	>250.00	–	>1.83
4k	186.67	12.58	>250.00	–	>1.34
4l	198.33	7.64	>250.00	–	>1.26
5	>250.00	–	>250.00	–	–
8a	79.00	7.94	65.33	8.39	0.83
8b	12.50	0.71	216.67	62.12	17.33
8c	>250.00	–	>250.00	–	–
8d	3.63	0.81	141.67	7.64	39.03
8e	23.67	6.66	143.33	44.81	6.06
8f	>250.00	–	>250.00	–	–
8g	65.67	4.04	102.33	10.79	1.56
8h	>250.00	–	>250.00	–	–
8i	>250.00	–	>250.00	–	–
8j	103.33	2.89	>250.00	–	>2.42
8k	>250.00	–	>250.00	–	–
7	>250.00	–	>250.00	–	–
8l	13.75	1.77	>250.00	–	>18.18
8m	21.50	0.71	198.33	2.89	9.23
8n	82.50	3.54	88.33	2.89	1.07
8o	38.50	12.02	189.67	4.51	4.93
8p	>250.00	–	>250.00	–	–
8q	>250.00	–	>250.00	–	–
8r	93.33	2.89	181.67	7.64	1.95
8s	>250.00	–	>250.00	–	–
8t	>250.00	–	>250.00	–	–
8u	98.33	5.77	>250.00	–	>2.54
8v	>250.00	–	>250.00	–	–
12	178.33	42.53	>250.00	–	>1.40
13a	67.33	6.43	95.67	4.04	1.42
13b	76.67	17.56	34.67	7.51	0.45
13c	>250.00	–	>250.00	–	–
13d	>250.00	–	>250.00	–	–
Cisplatin	27.33	6.81	–	–	–

Note: **A549**: Non-small lung cancer cell line; **L929**: Healthy mouse fibroblast cell line, **SD**: Standard deviation (±), and **SI**: Selectivity index (which is calculated as follows: IC_{50} on healthy cells/IC_{50} on cancer cells). All IC_{50} values are one-day cytotoxicity results. "–" means there are no meaningful results.

As proof of that, it was found that quinazoline analogue, quinolines (**13**) causes a decrease in anticancer activity. It is suggested that the azole rings attached to the sulfur atom should be bulky such as benzothiazole. In addition, the substituent on these rings should not induce acidity or reduce lipophilicity.

Table 7. Apoptotic rates of the synthesized compounds.

Compound	Q1	Q2	Q3	Q4	Q2+Q4
Control	0.01	2.17	91.24	6.59	8.76
4g	0.14	10.12	68.78	20.96	31.08
4h	0.17	6.13	84.17	9.53	15.66
8b	0.16	63.82	22.16	13.86	77.68
8d	0.10	4.54	91.31	4.05	8.59
8e	0.01	2.14	93.33	4.52	6.66
8l	0.00	8.26	76.05	15.69	23.95
8m	0.05	8.53	84.78	6.64	15.17
8o	0.06	7.52	85.91	6.51	14.03
Cisplatin	0.10	10.45	78.29	11.16	22.61

Note: **Q1**: Necrotic cells, **Q2**: Late apoptotic cells, **Q3**: Viable cells, **Q4**: Early apoptotic cells, **Q2+Q4**: Early and late apoptotic cells. A549 cells were used in this test.

Table 8. Inducing rate of the active compounds on caspase-3 enzyme.

Compound	+%	–%	Compound	+%	–%
Control	1.68	98.10	**8e**	5.70	93.73
4g	2.87	96.77	**8l**	49.10	49.55
4h	1.94	97.72	**8m**	31.79	66.75
8b	35.32	60.93	**8o**	20.63	78.46
8d	2.96	96.80	**Cisplatin**	34.39	63.13

Note: +%: Induced caspase-3 activity in cells and –%: Decreased caspase-3 activity in cells. Enzyme activity was determined using A549 cells.

Briefly, the findings indicated that novel eight quinazoline-based anticancer agents were discovered, four of them showed EGFR inhibition at one-digit an nM concentration.

3. SAR Summary

The structure–activity relationship of each compound has been explained individually in the related section of targets while here it was summarized and generalized them altogether. In **Figure 12**, virtualizing was built up to easily look at structural differences and their effects on anticancer activity and mechanisms of action.

Table 9. Results of mitochondrial membrane polarization% and depolarization% of active compounds.

Compound	polarization%[a)]	depolarization[a)]
Control	95.64	4.00
4g	83.55	15.41
4h	84.72	14.48
8b	24.27	75.30
8d	37.88	61.62
8e	66.84	28.96
8l	3.92	96.13
8m	15.87	83.70
8o	13.50	86.14
Cisplatin	62.86	36.01

[a)] Mitochondrial membrane polarization and depolarization was determined using A549 cells.

Table 10. Results of EGFR inhibition.

Compound	IC_{50} [nM]
4g	27588 ± 6.945
4h	5.298 ± 0.164
8b	>50000
8d	5.46 ± 0.221
8e	52.41 ± 2.312
8l	2.670 ± 0.124
8m	2.191 ± 0.908
8o	33657 ± 8.512
Gefitinib	4.169 ± 0.156

Note: For each compound, tests were repeated for four times.

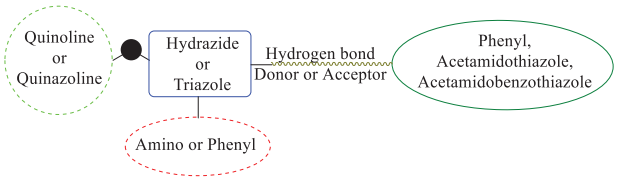

Figure 12. Diagram of structure–activity relationship.

According to that,

§ Anticancer effect of quinazoline derivatives was determined to be higher compared to quinoline derivatives.

§ Upon investigating all three different quinazolin-4(*3H*)-one series, the presence of a halogen group or a non-substituted aryl ring significantly enhances the anticancer activity. Although when the presence of an azole ring in the center increases the activity, the anticancer activity is similar when this structure is substituted with hydrazide. However, this replacement is thought to affect the activation pathway. It suggested that the presence of azole (specifically triazole) is more suitable for EGFR inhibition and caspase-3 activation.

§ Comparing the structures with bulk group/small group attached to the central ring (triazole), no significant difference between their anticancer potency was observed. However, the presence of the small group (NH_2) is more valuable for EGFR inhibition and caspase-3 activation.

§ The presence of a methyl bridge connecting the rings has been identified as a major point since it allows molecules to rotate and adapt to the binding region of proteins. Thus, it is suggested that sp^3 atom is essential to anticancer activity.

§ Benzothiazoles are found more favorable than thiazole ring system. The presence of bulky groups (benzothiazoles) increase stability as they can interact with peripheral amino acids, even when exposed to the effects of organic and inorganic solvents. Therefore, benzothiazoles play an important role in maintaining the stability of the ligand–enzyme complex. It is suggested that the major contribution of the benzothiazole ring to the activity is closely related to the solubility property of the structure. Therefore, any modifications made to this ring should be directed towards updating this property, not binding to the amino acid.

§ The presence of a hydrogen acceptor/donor group in the bridge between (benz)azole and central ring or hydrazide has an essential role on EGFR inhibition (by binding with Asp855, the allosteric amino acid) and caspase-3 activation (by binding with loop amino acids such as Arg64 or Arg207).

4. Conclusion

In this study, 11 pharmacophore hypotheses were developed using two different methods to define hit molecules for NSCLC by inhibiting EGFR. After screening in-house databank, the hits and their analogs were synthesized and analyzed. A total of 41 original substances, 37 final products and four intermediates, were subjected to MTT assay for their cytotoxicity effects on A549 and L929 cell lines. Apoptosis effects (between 6.66% and 77.68%), caspase-3 activation effects (1.94%–49.10%), mitochondrial membrane depolarization effects (14.48%–96.13%), and EGFR inhibition effects (2.191×10^{-9} M–50.00×10^{-6} M) of the most selective and active molecules were investigated. In the end, molecular docking studies were applied to understand the binding mode of the active compounds to the relevant protein while molecular dynamics simulation methods were used to examine the change of the interaction stability under the effect of time and environmental factors. After the effects of biological profile were determined in vitro and in silico approaches, novel eight quinazoline-based anticancer molecules (**4g**, **4h**, **8b**, **8d**, **8e**, **8l**, **8m**, and **8o**) were discovered, four of them (**4h**, **8d**, **8l**, and **8m**) showed significant EGFR inhibition. These eight compounds also showed good apoptosis-inducer profile via intrinsic and extrinsic pathways. In silico findings indicated that the quinazoline ring and acetamide moiety play a determined role in binding the proteins' active pocket since they stabilize the protein–ligand complex. In addition, in line with the findings obtained in this study, the structure-activity relationship for both protein-specific and general anticancer activity was presented and discussed. For further studies, formulation studies are scheduled to be performed, and the most potent compounds (**4h**, **8d**, **8l**, and **8m**) be investigated via in vivo methods.

5. Experimental Section

Developing Pharmacophore Hypotheses: A scientifical hypothesis should be reperformed and must be trustable. Therefore, the validation of the hypothesis is an essential step. For that, EF (enrichment coefficient), BEDROC (Boltzmann's enhanced receiver-operation properties), AUAC (area under the accumulation curve), ROC (receiver-operation properties), and RIE (initial enhancement) values of the hypothesis were first examined, and if they are appropriate, then that hypothesis can be used. According to literature,[53–56] those values should be as the following statements:

✓ EF value > 1 indicates that the hypothesis is working. The degree to which it is more than 1 indicates how many times a true active molecule is more likely to be instead of pseudo-active and inactive molecules, that is, indicating how strong the hypothesis is.
✓ BEDROCK ($\alpha = 20.0$) > 80% is essential to use the hypothesis.
✓ AUAC is a value used to validate the hypothesis. Simply put, AUAC means the ratio of false positives to active ingredients. In a well-distributed dataset, the probability of any randomly selected compound being active is expected to be higher than the false-positive probability. In short, this area reveals the discriminating power of the hypothesis, and the closer the value is to 1, the higher the discriminating power of the hypothesis.

Table 11. Indexing of interactions between active compounds and caspase-3 enzyme.

Compound	Moiety	Residue	Number and type of interaction
8b	Quinazoline H_6	Ser120	1, Ar H-bond
	Benzothiazole chloro	Trp206	1, halogen bond
	Acetamide nitrogen	Arg207	1, salt bridge
	Acetamide oxygen	Arg207	1, H-bond
	Benzothiazole H_7	Arg207	1, Ar H-bond
	Triazole N_1	Arg207	1, H-bond
	Quinazoline ring	Arg207	1, π–cation
	Benzothiazole chloro	Trp214	1, Halogen bond
	Benzothiazole chloro	Phe250	1, halogen bond
8l	Acetamide oxygen	Arg64	1, H-bond
	Acetamide nitrogen	Arg64	1, salt bridge
	Benzothiazole ring	Hie121	2, π–π stacking
	Benzothiazole H_4	Gly122	1, Ar H-bond
	Benzothiazole nitrogen	Gly122	1, H-bond
	Acetamide oxygen	Gln161	1, H-bond
	Benzothiazole nitrogen	Cys163	1, H-bond
	Benzothiazole ring	Tyr204	1, π–π stacking
	Triazole ring	Tyr204	1, π–π stacking
	Acetamide oxygen	Arg207	1, H-bond
	Quinazoline ring	Phe256	2, π–π stacking
8m	Acetamide oxygen	Arg64	1, H-bond
	Benzothiazole ring	Hie121	2, π–π stacking
	Benzothiazole H_4	Gly122	1, Ar H-bond
	Benzothiazole nitrogen	Gly122	1, H-bond
	Benzothiazole H_5	Glu123	1, Ar H-bond
	Benzothiazole ring	Tyr204	1, π–π stacking
	4-amino-1,2,4-triazole nitrogen hydrogen	Ser205	1, H-bond
	Acetamide oxygen	Arg207	1, H-bond
	Quinazoline ring	Phe256	2, π–π stacking
8o	Acetamide oxygen	Arg64	1, H-bond
	Benzothiazole ring	Hie121	1, π–π stacking
	Benzothiazole H_6	Gly122	1, aromatic H-bond
	Benzothiazole nitrogen	Gly122	1, H-bond
	Benzothiazole H_5	Glu123	1, aromatic H-bond
	Benzothiazole ring	Tyr204	1, π–π stacking
	4-amino-1,2,4-triazole nitrogen hydrogen	Ser205	1, H-bond
	Acetamide oxygen	Arg207	2, H-bond
	Quinazoline ring	Phe256	1, π–π stacking

✓ ROC value is an indicator of the discriminating power of the hypothesis, and the closer it is to 1, the stronger the hypothesis.
✓ RIE value, like AUAC, is an indicator of the discriminating power of the hypothesis and being above 1 is the minimum condition for the hypothesis to be used.

Above values were used to check all pharmacophore hypothesis. All these processes were carried out using the Maestro package program,[57] while the generation and validation of pharmacophore hypotheses were performed using the PHASE[58,59] module.

After obtaining hypotheses using the approaches described below, they were used together in the screening of the in-house molecular library which include novel 544 compounds containing quinoline and/or quinazoline nuclei. Any compound that matched with at least five hypothetical features was labeled as a lead molecule.

Developing Hypothesis Using Multiple Drugs and One Protein Crystal: Since the EGFR pathway was identified as the main target, the crystal structure of this protein (PDBID: 2ITY) was downloaded from the RCSB protein database.

Fourteen EGFR inhibitory drugs have been used as the active set (-tinibs: crizotinib, sunitinib, bosutinib, dasatinib, cabozantinib, dacomitinib, lapatinib, afatinib, brigatinib, ibrutinib, osimertinib, erlotinib, gefitinib, and neratinib), while 19 other kinases were used as inactive set because they were either reported with low efficiency or they are not binding at all to EGFR (-tinibs: imatinib, tofacitinib, nilotinib, ponatinib, lenvatinib, axitinib, alectinib, ruxolitinib, fostamatinib, baricitinib, cobimetinib,

Table 12. Indexing of interactions between active compounds and EGF receptor.

Compound	moiety	Residue	Number and type of interaction
4h	Sulfur of thiocarbonyl	Lys745	1, H-bond
	Quinazoline H_2	Gln791	1, Ar H-bond
	Quinazoline N_1	Met793	1, H-bond
	Quinazoline H_8	Met793	1, Ar H-bond
	Chloro of phenyl	Arg841	2, Halogen bond
	H of N_2 of hydrazine	Thr854	1, H-bond
	Phenyl H_2	Arg855	1, Ar H-bond
8d	Acetamide nitrogen	Lys745	1, salt bridge
	Methoxy oxygen	Cys797	1, H-bond
	Phenyl H_3	Arg841	1, Ar H-bond
	Phenyl ring	Arg841	1, π-cation
	Phenyl H_2	Arg855	1, Ar H-bond
8l	Acetamide oxygen	Lys745	1, H-bond
	Acetamide nitrogen	Lys745	1, salt bridge
	Quinazoline H_2	Gln791	1, Ar H-bond
	Quinazoline N_1	Met793	1, H-bond
	Quinazoline H_8	Met793	1, Ar H-bond
	Benzothiazole ring	Arg841	1, salt bridge
	Benzothiazole nitrogen	Arg841	1, H-bond
	4-amino-1,2,4-triazole nitrogen hydrogen	Asp855	1, H-bond
8m	Benzothiazole H_7	Ser720	1, Ar H-bond
	Acetamide nitrogen	Lys745	1, H-bond
	Acetamide nitrogen	Lys745	1, salt bridge
	Quinazoline H_2	Gln791	1, Ar H-bond
	Quinazoline N_1	Met793	1, H-bond
	Quinazoline H_8	Met793	1, Ar H-bond
	Benzothiazole ring	Arg841	2, π-cation
	4-amino-1,2,4-triazole nitrogen hydrogen	Arg855	1, H-bond

ceritinib, binimetinib, lorlatinib, gilteritinib, erdafitinib, acalabrutinib, pexidartinib, and larotrectinib). Therefore, a total of 33 inhibitors, known as anticancer agents, were used to develop a series of pharmacophore hypotheses.

Docking studies of these 33 tinibs drugs were performed using similar procedures,[50,60–62] and the best poses were selected for the next step. Based on these selected poses, hypothesis development studies were carried out using multiple molecules and a single EGFR protein crystal. Later, the generated hypotheses were validated using all tyrosine kinase (-tinib compounds) and the fragment collection which is freely offered by Schrodinger LLC (accessed 09.09.2020). The validation process followed the description provided in Section 5.1.

Developing Hypotheses Using Literature-Based EGFR Active Compounds and Single Protein Crystal: A total of 5947 compounds reported for their EGFR inhibition pKi value were downloaded from the ZINC database (https://zinc.docking.org/ accessed: 29.08.2020). Then, compounds containing pyridine or pyrimidine rings with at least three substitutions were filtered. Using the Maestro program,[57] the selected compounds were prepared in accordance with the pH = 7.4 ± 1.0 using LigPrep module. Following this step, all subsequent procedures for hypothesis generation and validation remained identical to the above-described methods (Section 5.1.1), with the exception of a minor change, which is descripted as follows:

- Compounds with a value of pKi of 7.0 and above were categorized as active compounds, while the remaining compounds were considered neutral and included in the hypothesis without any assignment. (They have not been removed since those compounds have not yet been tested in clinical practice.)
- The molecules used for the trap set is a set of 1000 molecules obtained from Schrodinger LLC (accessed on 30.08.2020), which were specially prepared for its drug-like properties.[63,64] Following the generation hypotheses, their validations were made as descripted in Section 5.1.

Chemistry: All chemicals were purchased from Sigma-Aldrich Chemical Co. (Sigma-Aldrich Corp., St. Louis, MO) and Merck Chemicals (Merck KGaA, Darmstadt, Germany). Melting points (m.p.) were determined by MP90 digital melting point apparatus (Mettler Toledo, Ohio, USA) and were reported without correction. Reactions were monitored by thin-layer chromatography (TLC) using Silica Gel 60 F254 TLC plates (Merck KGaA, Darmstadt, Germany). Spectroscopic data were recorded with the following instruments: ^{1}H-NMR (nuclear magnetic resonance) Bruker DPX-300 FT-NMR spectrometer, ^{13}C-NMR, Bruker DPX 75 MHz spectrometer (Bruker Bioscience, Billerica, MA); mass (HRMS) spectra were recorded on a liquid chromatography connected with hybrid ion-trap and time-of-flight mass spectrometry (Shimadzu) using electrospray ionization. The synthesis route of the target molecules is illustrated in Scheme 1.

Synthesis of 4(3H)-Quinazolinone (1): Two methods were used to obtain the title compound. In Method A, anthranilic acid (1 eq) and formamide (1.2 eq) were stirred in an oil bath. The end of the reaction was checked with TLC. Upon completion, the reaction mixture was poured into iced water, then the solid phase was washed with water while filtering. In

Method B, anthranilic acid (1 eq) and formamide (1.2 eq) were reacted under 500 W and 220 °C in a microwave tank for 15 min. Similar to Method A, the reaction was controlled via TLC, and the same finalization procedure as in method A was followed. Both products were subsequently crystallized from ethanol (Scheme 1a).

Synthesis of Ethyl 2-[4-Oxoquinazolin-3(4H)-yl]acetate (2) and ethyl 2-(Quinolin-8-yloxy)Acetate (9): 4(3*H*)-Quinazolinone (**1**) or 8-hydroxyquinoline was dissolved in acetone and 1.5 equivalent moles of K_2CO_3 was added to the reaction flask. Then ethyl 2-bromoacetate (1.1 eq mole) was added and the mixture was refluxed for 18 h. The reactions were controlled via TLC, and then acetone was evaporated. The resulting solid phases were washed with water while filtering. The dry products were subsequently crystallized from hexane (Scheme 1b).

Synthesis of 2-[4-Oxoquinazolin-3(4H)-yl]Acetohydrazide (3) and 2-(Quinolin-8-yloxy) Acetohydrazide (10): Compound **2** or compound **9** (1 eq.) was dissolved in ethanol. Hydrazine mono hydrate (1.5 eq.) in ethanol solution was added slowly into solution. The solution was stirred over the night and the reaction was controlled via TLC. After completion of the reaction, the solid was filtered. Final products were recrystallized from absolute ethanol (Scheme 1c).

Synthesis of Target Products N-(Substituted)-2-{2-[4-Oxoquinazolin-3(4H)-yl]acetyl}hydrazine-1-Carbothioamide Derivatives (4a-4l) and the Intermediate Compound N-(4-Methoxyphenyl)-2-[2-(Quinolin-8-yloxy)acetyl]hydrazine-1-Carbothioamide (11): In an ice bath, equal moles of various alkyl/aryl isothiocyanates dissolved in ethanol are added into 2-[4-oxoquinazolin-3(4*H*)-yl]acetohydrazide (**3**) in ethanol solution or 4-methoxyphenylisothiocyanate in ethanol solution was added into 2-(quinolin-8-yloxy)acetohydrazide (**10**) slowly. The mixtures were stirred over a day and the reactions were controlled via TLC. The solid was filtered and the final products were recrystallized from absolute ethanol (Scheme 1d). Compounds **4a–4l** and **11** are displayed in Table 4.

Synthesis of 3-{[4-(4-Methoxyphenyl)-5-thioxo-4,5-Dihydro-1H-1,2,4-triazole-3-yl]methyl}quinazolin-4(3H)-one (5) and 4-(4-Methoxyphenyl)-5-[(quinolin-8-yloxy)methyl]-4H-1,2,4-triazole-3-thiol (12): Compounds **4a** or **11** dissolved in 2 M sodium ethoxide (NaOEt) solution and refluxed. The reactions were controlled via TLC. The mixtures were poured into iced water and the pH of the mixtures was set to 7. The solid phase was filtered and washed with water. These intermediates were recrystallized from absolute ethanol (Scheme 1e).

Synthesis of 3-[(5-thioxo-4,5-dihydro-1,3,4-oxadiazol-2-yl)methyl]Quinazolin-4(3H)-one (6): In an ice bath, compound **3** (1 eq) dissolved in 2 M sodium ethoxide (NaOEt) solution, then CS_2 (1.1 eq) was carefully added to the solution. The mixture was stirred at room temperature for 30 min. After precipitation, it was refluxed under reflux for 2 h. The reaction was finished according to TLC. The mixture was poured into iced water and the pH was adjusted to 7 with 9.8% HCl solution. The precipitate was filtered and washed with water. The final product was recrystallized from ethanol (Scheme 1f).

3-[(4-Amino-5-thioxo-4,5-Dihydro-1H-1,2,4-triazole-3-yl)methyl)Quinazolin-4(3H)-one (7): Hydrazine monohydrate (1.5 eq) was added to solution of compound **6** (1 eq) in ethanol, then it was refluxed for 2 h. The reaction was controlled with TLC. After completion of the reaction, the precipitate was filtered and washed with ethanol. The crude product was recrystallized from alcohol (Scheme 1g).

Synthesis of Final Products 2-{[4-(4-Methoxyphenyl/amino)-5-{[4-Oxoquinazolin-3(4H)-yl]methyl}-4H-1,2,4-triazole-3-yl]thio}-N-aryl Acetamide (8a–8k;81–8v) and 2-({4-[4-Methoxyphenyl]-5-[(Quinolin-8-yloxy)methyl]-4H-1,2,4-Triazole-3-yl}thio)-N-aryl Acetamide (13a–13d): Compounds **5**, **7**, or **12** were stirred with equal moles of 2-chloro-N-aryl acetamide derivatives in acetone media with K_2CO_3 (1.5 eq) at room temperature for 2 h. The reactions were controlled according to TLC. After completion of the reactions, the solvents were evaporated, and the remaining phases were filtered and washed with water. The crude products were crystallized from absolute ethanol (Scheme 1h). Compounds **8a–8v** and **13a–13d** are displayed in Table 5.

Experimental Activity Studies—MTT Tests: MTT tests were performed the same as in previous studies.[60,61,65,66] Non-small cell lung cancer cell line (A549-ATCC CCL-185) was used to determine anticancer activity and healthy mouse fibroblast cell line (L-929 ATCC CCL-1TM) was used to determine cytotoxicity on healthy cells.

Determination of Apoptotic Effects: Apoptosis and necrosis are cell death scenarios known as natural and cancerous tissue death, i.e., natural death and suicide of the cell, respectively. For this reason, one of the important points that is expected from anticancer drugs is to induces the death of cancer cells in an apoptotic way. To determine this, it was investigated that whether active compounds with high selectivity index to A549 cells induce apoptosis. FITC Annexin V apoptosis detection kit (BD Pharmingen, San Jose, CA) kit was used and the method used in this research was carried out the same as in previously published articles.[60,67]

Mechanism of Action Studies: Determination of Caspase-3 Activation: In this study, the determination of caspase-3 activity was performed the same as in a previous studies.[68–70]

Determination of Mitochondrial Membrane Depolarization: The determination of mitochondrial membrane depolarization is based on staining cells with JC-1 and the method for this study was performed according to the supplier's instructions (BD, Pharmingen Flow cytometry kit) and another previous study.[71] After the determination of the most active compounds by the MTT method, the mitochondrial membrane integrity of the compounds on A549 cells was tested at their IC_{50} concentrations. Also, cells were analyzed using flow cytometry. The obtained results were compared using cisplatin as the positive control.

Determination of EGFR Inhibition Activity: EGFR (ErbB-1; HER1) is from the receptor tyrosine kinase family and was reported to be associated with cancer in various tissues due to its overexpression or hyperactivation as mentioned several times.[18–24] The EGFR kinase assay kit (BPS Bioscience, Cat. No. 40321, San Diego, CA) was used according to the manufacturer's instructions to determine the EGFR kinase inhibition of the active molecules. Four independent experiments were performed for each compound, and the mean and standard deviation values were calculated. Gefitinib was used as the positive control.

Molecular Docking and Dynamics Simulation Studies: Molecular docking studies are in silico procedures applied to understand the binding mode between protein and active molecules. The X-ray crystal structures of caspase-3 (PDB ID: 4QTX) and EGFR (PDB ID: 2ITY) were downloaded from the Protein Data Bank server (www.pdb.org, accessed 01 Aug 2019). The structures of these proteins were individually constructed using the Schrödinger Maestro[57] interface and then prepared in the Protein Preparation Wizard protocol of Schrödinger Suite 2020. The pH value of the compounds was set to 7.4 ± 1.0 which was prepared using the LigPrep module.[72] The mapping of the binding sites was generated using the Glide module,[73] and the calculations were performed using the standard precision method (SP).

Molecular dynamics studies were performed by using the same procedures reported in previous studies.[41,50,74–76] Active compounds and their proteins were prepared separately to obtain system setup using "System Setup" module in Desmond application.[77] Transferable intermolecular potential with three points water model was used for the creation of the hydration model. POPC (1-Palmitoyl, 2-oleoylphosphatidylcholine) membrane[78,79] model was preferred during the system preparation. The neutralization of the system was achieved using Na^+ and Cl^- ions. The molecular dynamics simulation was performed following the completion of the system setup.

Supporting Information

Supporting Information is available from the Wiley Online Library or from the author.

Acknowledgements

The authors thank the MERLAB Laboratory, Anadolu University. This study was supported by Anadolu University (Funding No. 2107S116). For some final compounds, the authors have applied to Turkish Patent and Trademark Office, Application No. 2023/002077 and Reference No. 21699/1.

Ethics Approval and Consent to Participate

Not applicable.

Conflict of Interest

The authors declare no conflicts of interest.

Author Contributions

L.Y. and A.E.E.: conceptualization; A.E.E.: methodology and software; L.Y., A.E.E., and G.A.-Ç.: validation; A.E.E.: formal analysis; A.E.E., B.N.S., and G.A.-Ç.: investigation; L.Y. and G.A.-Ç.: resources; L.Y. and A.E.E.: data curation; A.E.E. and G.A.-Ç.: writing—original draft preparation; L.Y.: writing—review and editing; A.E.E., B.N.S., and G.A.-Ç.: visualization; L.Y. and G.A.-Ç.: supervision. All authors have approved the final article should be true and included in the disclosure.

Data Availability Statement

All analyze data were shared in supplementary file. MDS videos can be watched via these links (Video 1: https://youtu.be/lvf-9HGHPZg, Video2: https://youtu.be/L80wa2w7CH8).

Keywords

anticancer, EGFR, molecular dynamics simulation, pharmacophore hypothesis, quinazolin-4(3H)-one

Received: August 5, 2024
Revised: September 26, 2024
Published online: October 18, 2024

[1] D. M. Hausman, *Perspect. Biol. Med.* **2019**, *62*, 778.
[2] D. A. Kooby, *J. Surg. Oncol.* **2017**, *116*, 470.
[3] C. Allen, S. Her, D. A. Jaffray, *Adv. Drug Delivery Rev.* **2017**, *15*, 1.
[4] S. P. Gupta, A. Sharma, V. M. Patil, *Anti-Cancer Agents Med. Chem.* **2021**, *21*, 1638.
[5] J. van den Bulk, E. M. Verdegaal, N. F. de Miranda, *Open Biol.* **2018**, *8*, 180037.
[6] N. L. Stout, J. Baima, A. K. Swisher, K. M. Winters-Stone, J. Welsh, *PM R* **2017**, *9*, S347.
[7] F. E. Azar, S. Azami-Aghdash, F. Pournaghi-Azar, A. Mazdaki, A. Rezapour, P. Ebrahimi, N. Yousefzadeh, *BMC Health Serv. Res.* **2017**, *17*, 413.
[8] M. B. Schabath, M. L. Cote, *Cancer Epidemiol., Biomarkers Prev.* **2019**, *28*, 1563.
[9] F. Z. Wu, P. L. Kuo, Y. L. Huang, E. K. Tang, C. S. Chen, M. T. Wu, Y. P. Lin, *Sci. Rep.* **2019**, *9*, 19386.
[10] E. Jakobsen, K. E. Olsen, M. Bliddal, M. Hornbak, G. F. Persson, A. Green, *BMC Cancer* **2021**, *21*, 985.
[11] N. M. Namee, L. O'Driscoll, *Biochim. Biophys. Acta, Rev. Cancer* **2018**, *1870*, 123.
[12] M. M. Gottesman, *Annu. Rev. Med.* **2002**, *53*, 615.
[13] S. Hussain, A. Singh, S. U. Nazir, S. Tulsyan, A. Khan, R. Kumar, N. Bashir, P. Tanwar, R. Mehrotra, *J. Cell. Biochem.* **2019**, *120*, 14213.
[14] Z. F. Lim, P. C. Ma, *J. Hematol. Oncol.* **2019**, *12*, 134.
[15] S. Naghizadeh, A. Mohammadi, B. Baradaran, B. Mansoori, *Gene* **2019**, *714*, 143972.
[16] N. S. Akins, T. C. Nielson, H. V. Le, *Curr. Top. Med. Chem.* **2018**, *18*, 494.
[17] M. A. Olayioye, R. M. Neve, H. A. Lane, N. E. Hynes, *EMBO J.* **2000**, *19*, 3159.
[18] M. Westphal, C. L. Maire, K. Lamszus, *CNS Drugs* **2017**, *31*, 723.
[19] A. Dokala, S. S. Thakur, *Oncogene* **2017**, *36*, 2337.
[20] M. M. Moasser, *Oncogene* **2007**, *26*, 6577.
[21] C. E. Geyer, J. Forster, D. Lindquist, S. Chan, C. G. Romieu, T. Pienkowski, A. Jagiello-Gruszfeld, J. Crown, A. Chan, B. Kaufman, *N. Engl. J. Med.* **2006**, *355*, 2733.
[22] M. A. S. Abourehab, A. M. Alqahtani, B. G. M. Youssif, A. M. Gouda, *Molecules* **2021**, *26*, 6677.
[23] P. Diz Taín, A. L. González, A. García-Palomo, *Med. Clín.* **2016**, *146*, 7.
[24] N. Normanno, M. R. Maiello, A. De Luca, *J. Cell. Physiol.* **2003**, *194*, 13.
[25] Y. Jia, C. H. Yun, E. Park, D. Ercan, M. Manuia, J. Juarez, C. Xu, K. Rhee, T. Chen, H. Zhang, S. Palakurthi, J. Jang, G. Lelais, M. DiDonato, B. Bursulaya, P. Y. Michellys, R. Epple, T. H. Marsilje, M. McNeill, W. Lu, J. Harris, S. Bender, K. K. Wong, P. A. Janne, M. J. Eck, *Nature* **2016**, *534*, 129.
[26] A. Ayati, S. Moghimi, M. Toolabi, A. Foroumadi, *Eur. J. Med. Chem.* **2021**, *221*, 113523.
[27] R. Bolteau, R. Duroux, A. Laversin, B. Vreulz, A. Shiriaeva, B. Stauch, G. W. Han, V. Cherezov, N. Renault, A. Barczyk, S. Ravez, M. Coevoet, P. Melnyk, M. Liberelle, S. Yous, *Eur. J. Med. Chem.* **2022**, *241*, 114620.
[28] R. M. Borik, M. A. Hussein, *Curr. Pharm. Biotechnol.* **2022**, *23*, 1179.
[29] M. A. Alossaimi, Y. Riadi, M. H. Geesi, E. H. Anouar, M. K. Aldhafiri, A. I. Alanazi, O. Dehbi, E. O. Ibnouf, R. Azzallou, *J. Mol. Struct.* **2022**, *1266*, 133519.
[30] Y. Liang, H. Zhang, X. Zhang, Y. Peng, J. Deng, Y. Wang, R. Li, L. Liu, Z. Wang, *Bioorg. Chem.* **2022**, *127*, 105981.
[31] T. H. Qin, J. C. Liu, J. Y. Zhang, L. X. Tang, Y. N. Ma, R. Yang, *Bioorg. Med. Chem. Lett.* **2022**, *72*, 128877.
[32] R. A. Wagdy, P. J. Chen, M. M. Hamed, S. S. Darwish, S. H. Chen, A. H. Abadi, M. Abdel-Halim, T. L. Hwang, M. Engel, *Bioorg. Chem.* **2022**, *127*, 105977.
[33] C. Hanwarinroj, P. Thongdee, D. Sukchit, S. Taveepanich, P. Kamsri, A. Punkvang, S. Ketrat, P. Saparpakorn, S. Hannongbua, K. Suttisintong, P. Kittakoop, J. Spencer, A. J. Mulholland, P. Pungpo, *J. Mol. Graphics Modell.* **2022**, *115*, 108231.
[34] C. Muller, V. Tilloy, E. Frobert, L. Feghoul, I. Garrigue, Q. Lepiller, A. Mirand, E. Sidorov, S. Hantz, S. Alain, *Antiviral Res.* **2022**, *204*, 105361.
[35] S. E. S. Abbas, N. M. Abdel-Gawad, R. F. George, M. G. A. Elyazid, M. A. Zaater, M. K. El-Ashrey, *J. Mol. Struct.* **2022**, *1269*, 133851.
[36] C. Hauguel, S. Ducellier, O. Provot, N. Ibrahim, D. Lamaa, C. Balcerowiak, B. Letribot, M. Nascimento, V. Blanchard, L. Askenatzis, H. Levaique, J. Bignon, F. Baschieri, C. Bauvais, G. Bollot, D. Renko, A. Deroussent, B. Prost, M. C. Laisne, S. Michallet, L. Lafanechere, S. Papot, G. Montagnac, C. Tran, M. Alami, S. Apcher, A. Hamze, *Eur. J. Med. Chem.* **2022**, *240*, 114573.
[37] T. Wu, Q. Qin, R. Lv, N. Liu, W. Yin, C. Hao, Y. Sun, C. Zhang, Y. Sun, D. Zhao, M. Cheng, *Eur. J. Med. Chem.* **2022**, *238*, 114451.
[38] Z. Liang, Y. Wang, H. Zhang, J. Deng, F. Lei, J. Li, T. Shi, S. Wang, R. Li, Z. Wang, *Eur. J. Med. Chem.* **2022**, *239*, 114530.
[39] M. Menna, F. Fiorentino, B. Marrocco, A. Lucidi, S. Tomassi, D. Cilli, M. Romanenghi, M. Cassandri, S. Pomella, M. Pezzella, D. Del Bufalo, M. S. Zeya Ansari, N. Tomasevic, M. Mladenovic, M. Viviano, G. Sbardella, R. Rota, D. Trisciuoglio, S. Minucci, A. Mattevi, D. Rotili, A. Mai, *Eur. J. Med. Chem.* **2022**, *237*, 114410.
[40] F. Lei, Y. Xiong, Y. Wang, H. Zhang, Z. Liang, J. Li, Y. Feng, X. Hao, Z. Wang, *J. Med. Chem.* **2022**, *65*, 7975.
[41] A. E. Evren, A. B. Karaduman, B. N. Saglik, Y. Ozkay, L. Yurttas, *ACS Omega* **2023**, *8*, 1410.

[42] L. Yurttas, B. Demir, G. A. Ciftci, *Anti-Cancer Agents Med. Chem.* **2018**, *18*, 1115.
[43] L. Yurttaş, A. Kubilay, A. E. Evren, İ. Kısacık, H. K. Gençer, *Phosphorus, Sulfur Silicon Relat. Elem.* **2020**, *195*, 767.
[44] Z. Liu, X. Zhang, H. Zhang, H. Jiang, X. Zhao, L. Shi, X. Zhu, X. Hao, M. Song, *Chin. J. Org. Chem.* **2020**, *40*, 2755.
[45] G. M. Schroeder, Y. An, Z. W. Cai, X. T. Chen, C. Clark, L. A. Cornelius, J. Dai, J. Gullo-Brown, A. Gupta, B. Henley, J. T. Hunt, R. Jeyaseelan, A. Kamath, K. Kim, J. Lippy, L. J. Lombardo, V. Manne, S. Oppenheimer, J. S. Sack, R. J. Schmidt, G. Shen, K. Stefanski, J. S. Tokarski, G. L. Trainor, B. S. Wautlet, D. Wei, D. K. Williams, Y. Zhang, Y. Zhang, R. M. Borzilleri, *J. Med. Chem.* **2009**, *52*, 1251.
[46] E. J. Griffiths, in *Advances in Mitochondrial Medicine* (Eds: R. Scatena, B. P. B. Giardina), Springer, Dordrecht, Netherlands **2012**, p. 459.
[47] J. Lopez, S. W. Tait, *Br. J. Cancer* **2015**, *112*, 957.
[48] T. F. Che, C. W. Lin, Y. Y. Wu, Y. J. Chen, C. L. Han, Y. L. Chang, C. T. Wu, T. H. Hsiao, T. M. Hong, P. C. Yang, *Oncotarget* **2015**, *6*, 37349.
[49] C. Cade, P. Swartz, S. H. MacKenzie, A. C. Clark, *Biochemistry* **2014**, *53*, 7582.
[50] A. E. Evren, D. Nuha, S. Dawbaa, B. N. Saglik, L. Yurttas, *Eur. J. Med. Chem.* **2022**, *229*, 114097.
[51] N. T. Yucel, D. Osmaniye, U. Kandemir, A. E. Evren, O. D. Can, U. D. Ozkay, *Molecules* **2021**, *26*, 3350.
[52] C. H. Yun, T. J. Boggon, Y. Li, M. S. Woo, H. Greulich, M. Meyerson, M. J. Eck, *Cancer Cell* **2007**, *11*, 217.
[53] J.-F. Truchon, C. I. Bayly, *J. Chem. Inf. Comput. Sci.* **2007**, *47*, 488.
[54] A. Ece, *J. Biomol. Struct. Dyn.* **2020**, *38*, 565.
[55] A. Maryam, R. R. Khalid, A. R. Siddiqi, A. Ece, *J. Biomol. Struct. Dyn.* **2021**, *39*, 2302.
[56] O. Dror, D. Schneidman-Duhovny, Y. Inbar, R. Nussinov, H. J. Wolfson, *J. Chem. Inf. Model.* **2009**, *49*, 2333.
[57] *Schrödinger Release 2020-3*, Maestro, Schrödinger, LLC, New York, NY, **2020**.
[58] S. L. Dixon, A. M. Smondyrev, E. H. Knoll, S. N. Rao, D. E. Shaw, R. A. Friesner, *J. Comput.-Aided Mol. Des.* **2006**, *20*, 647.
[59] S. L. Dixon, A. M. Smondyrev, S. N. Rao, *Chem. Biol. Drug Des.* **2006**, *67*, 370.
[60] A. E. Evren, L. Yurttas, B. Ekselli, G. Akalin-Ciftci, *Phosphorus, Sulfur Silicon Relat. Elem.* **2019**, *194*, 820.
[61] A. E. Evren, L. Yurttaş, B. Eksellı, G. Akalın-Cıftcı, *Lett. Drug Des. Discovery* **2019**, *16*, 547.
[62] D. Nuha, A. E. Evren, Z. S. Ciyanci, H. E. Temel, G. Akalin Ciftci, L. Yurttas, *Arch. Pharm.* **2022**, *355*, e2200105.
[63] R. A. Friesner, J. L. Banks, R. B. Murphy, T. A. Halgren, J. J. Klicic, D. T. Mainz, M. P. Repasky, E. H. Knoll, M. Shelley, J. K. Perry, D. E. Shaw, P. Francis, P. S. Shenkin, *J. Med. Chem.* **2004**, *47*, 1739.
[64] T. A. Halgren, R. B. Murphy, R. A. Friesner, H. S. Beard, L. L. Frye, W. T. Pollard, J. L. Banks, *J. Med. Chem.* **2004**, *47*, 1750.
[65] A. E. Evren, L. Yurttaş, B. Ekselli, O. Aksoy, G. Akalin-Çiftçi, *Lett. Drug Des. Discovery* **2021**, *18*, 372.
[66] L. Yurttas, B. K. Cavusoglu, G. A. Ciftci, H. E. Temel, *Anti-Cancer Agents Med. Chem.* **2018**, *18*, 914.
[67] L. Yurttas, S. Demirayak, G. A. Ciftci, *Anti-Cancer Agents Med. Chem.* **2015**, *15*, 1174.
[68] L. Yurttas, Y. Ozkay, G. Akalin-Ciftci, S. Ulusoylar-Yildirim, *J. Enzyme Inhib. Med. Chem.* **2014**, *29*, 175.
[69] G. A. Ciftci, A. Iscan, M. Kutlu, *Cytotechnology* **2015**, *67*, 893.
[70] L. Yurttas, G. A. Ciftci, H. E. Temel, B. N. Saglik, B. Demir, S. Levent, *Anti-Cancer Agents Med. Chem.* **2017**, *17*, 1846.
[71] N. P. Kumar, P. Sharma, T. S. Reddy, N. Shankaraiah, S. K. Bhargava, A. Kamal, *Eur. J. Med. Chem.* **2018**, *151*, 173.
[72] *Schrödinger release. 2020-3, LigPrep 2020*, Schrödinger, LLC, New York, NY, **2020**.
[73] *Schrödinger Release 2020-3*, Glide, Schrödinger, LLC, New York, NY, **2020**.
[74] S. Dawbaa, A. E. Evren, B. N. Saglik, N. Gundogdu-Karaburun, A. C. Karaburun, *Future Med. Chem.* **2022**, *14*, 1663.
[75] D. Osmaniye, A. E. Evren, B. N. Saglik, S. Levent, Y. Ozkay, Z. A. Kaplancikli, *Arch. Pharm.* **2022**, *355*, e2100450.
[76] N. T. Yucel, A. E. Evren, U. Kandemir, O. D. Can, *J. Psychopharmacol.* **2022**, *36*, 819.
[77] *Schrödinger Release 2020-3*, Desmond, Schrödinger, LLC, New York, NY, **2020**.
[78] A. C. Kalli, M. S. Sansom, R. A. Reithmeier, *PLoS Comput. Biol.* **2015**, *11*, e10041234123.
[79] K. B. Abd Halim, H. Koldso, M. S. P. Sansom, *Biochim. Biophys. Acta* **2015**, *1850*, 1017.